Title

Dysregulation of CD4+ and CD8+ resident memory T, myeloid, and stromal cells in steroid-experienced, checkpoint inhibitor colitis.

Journal

Journal for ImmunoTherapy of Cancer, 12(4)

Authors

He, Jun
Kim, Yang-Joon
Mennillo, Elvira
et al.

Publication Date

2024-04-19

DOI

10.1136/jitc-2023-008628

Journal for ImmunoTherapy of Cancer

Dysregulation of CD4$^+$ and CD8$^+$ resident memory T, myeloid, and stromal cells in steroid-experienced, checkpoint inhibitor colitis

Jun Yan He,[1] Yang-Joon Kim,[2] Elvira Mennillo,[3] Iulia Rusu,[3] Jared Bain,[3] Arjun A Rao,[4] Christopher Andersen,[4] Karen Law,[1] Hai Yang,[1] Jessica Tsui,[4] Alan Shen,[4] Brittany Davidson,[4] Divyashree Kushnoor,[4] Yimin Shi,[1] Frances Fan,[1] Alexander Cheung ,[1] Li Zhang,[1] Lawrence Fong,[1] Alexis J Combes,[3,4,5,6] Angela O Pisco,[2] Michael G Kattah,[3] David Y Oh [1]

To cite: He JY, Kim Y-J, Mennillo E, *et al*. Dysregulation of CD4$^+$ and CD8$^+$ resident memory T, myeloid, and stromal cells in steroid-experienced, checkpoint inhibitor colitis. *Journal for ImmunoTherapy of Cancer* 2024;**12**:e008628. doi:10.1136/jitc-2023-008628

► Additional supplemental material is published online only. To view, please visit the journal online (https://doi.org/10.1136/jitc-2023-008628).

MGK and DYO contributed equally.

Accepted 20 March 2024

For numbered affiliations see end of article.

Correspondence to
Dr David Y Oh;
David.Oh@ucsf.edu

Dr Michael G Kattah;
michael.kattah@ucsf.edu

ABSTRACT

Background Colitis caused by checkpoint inhibitors (CPI) is frequent and is treated with empiric steroids, but CPI colitis mechanisms in steroid-experienced or refractory disease are unclear.

Methods Using colon biopsies and blood from predominantly steroid-experienced CPI colitis patients, we performed multiplexed single-cell transcriptomics and proteomics to nominate contributing populations.

Results CPI colitis biopsies showed enrichment of CD4$^+$resident memory (RM) T cells in addition to CD8$^+$ RM and cytotoxic CD8$^+$ T cells. Matching T cell receptor (TCR) clonotypes suggested that both RMs are progenitors that yield cytotoxic effectors. Activated, CD38$^+$ HLA-DR$^+$ CD4$^+$ RM and cytotoxic CD8$^+$ T cells were enriched in steroid-experienced and a validation data set of steroid-naïve CPI colitis, underscoring their pathogenic potential across steroid exposure. Distinct from ulcerative colitis, CPI colitis exhibited perturbed stromal metabolism (NAD$^+$, tryptophan) impacting epithelial survival and inflammation. Endothelial cells in CPI colitis after anti-TNF and anti-cytotoxic T-lymphocyte-associated antigen 4 (anti-CTLA-4) upregulated the integrin $\alpha4\beta7$ ligand molecular vascular addressin cell adhesion molecule 1 (MAdCAM-1), which may preferentially respond to vedolizumab (anti-$\alpha4\beta7$).

Conclusions These findings nominate CD4$^+$ RM and MAdCAM-1$^+$ endothelial cells for targeting in specific subsets of CPI colitis patients.

WHAT IS ALREADY KNOWN ON THIS TOPIC

⇒ Checkpoint inhibitor (CPI) colitis involves CD8$^+$ resident memory (RM) T cells which may give rise to CD8$^+$ cytotoxic effectors, but the contribution of other pathogenic immune precursor populations, non-immune populations such as stroma, and distinct features of colitis caused by different CPI is unclear.

WHAT THIS STUDY ADDS

⇒ This study identifies: (1) CD4$^+$ RM cells as clonally related precursors for cytotoxic CD8$^+$ effectors, across steroid exposure; (2) stromal metabolic pathways that impact epithelial survival and inflammation distinct from ulcerative colitis (UC); (3) distinct cytotoxic and co-stimulatory pathways in anti--cytotoxic T-lymphocyte-associated antigen 4 (CTLA-4) versus anti-programmed cell death protein 1 (anti-PD-1) colitis; (4) anti-TNF and anti-CTLA-4-treated colitis patients that may selectively upregulate endothelial MAdCAM-1, which is the ligand for the integrin targeted by vedolizumab.

HOW THIS STUDY MIGHT AFFECT RESEARCH, PRACTICE OR POLICY

⇒ This work identifies novel precursors (CD4$^+$ RM) as additional targets for therapeutic intervention, and specific subsets of patients that may be more likely to respond to targeted use of vedolizumab, in CPI colitis.

BACKGROUND

Cancer immunotherapy with checkpoint inhibitors (CPI) blocking inhibitory programmed cell death protein 1 (PD-1) and cytotoxic T-lymphocyte-associated antigen 4 (CTLA-4), while highly effective, frequently induces colitis in up to 25% of patients receiving combination therapy.[1] This immune-related adverse event (IRAE) can interrupt effective therapy and preclude rechallenge. Our understanding of the pathogenic mechanisms of this disease state remains limited.

Recent work has taken a patient-centered approach, studying biopsies from endoscopically confirmed CPI colitis in patients, and subjecting these to biased and unbiased analyses (single cell and bulk sequencing, flow cytometry, and immunofluorescence).[2–4] While these studies have pointed to cytotoxic T-cell effectors and myeloid-related

inflammation downstream of interferon, their focus has been the steroid-naïve state[2] or the immune compartment.[2 4] Hence, the contribution of previously unidentified components of immune, and especially non-immune, cellular compartments is lacking. Additionally, studies focused on steroid-experienced patients are limited. This is also the population with the greatest clinical need, as current therapies after steroids are empiric (eg, anti-TNF or the anti-α4β7 antibody vedolizumab) and are not targeted to the treatment history and unique biology of these patients. Additionally, some steroid-refractory patients do not respond to these second-line therapies, highlighting the urgent need for novel therapeutic targets in this disease state.

Here we analyze an unbiased discovery cohort of predominantly steroid-experienced CPI colitis patients (eight steroid-experienced, one steroid-naïve), with single-cell genomic data from both immune and non-immune compartments, and multiple modalities of internal proteomic validation including cytometry by time-of-flight (CyTOF) and cellular indexing of transcriptomes and epitopes by sequencing (CITE-seq). We also validate against published single-cell studies of steroid-naïve CPI colitis to identify common and distinct mechanisms of disease. This work nominates important contributions of activated $CD4^+$ resident memory (RM) cells (in addition to known contributions of $CD8^+$ RM and cytotoxic effector populations), and homeostatic pathways in non-immune stromal populations impacting epithelial survival, to CPI colitis across the steroid exposure spectrum. We also identify subsets of steroid-experienced CPI colitis patients which may preferentially upregulate the vedolizumab target MAdCAM-1. This identifies specific patient subsets that may benefit from both existing and novel therapeutic approaches for this IRAE.

RESULTS

A multiomic workflow to study CPI colitis

To study checkpoint inhibitor-induced colitis (CPI colitis) through an unbiased, multiomic lens, we performed multiplexed single-cell RNA sequencing (scRNA-seq) and T cell receptor (TCR) sequencing (TCR-seq) (10x Genomics), with barcoded antibody staining for protein features (TotalSeq-C, BioLegend), on patient colon biopsies and peripheral blood mononuclear cells (PBMCs) from healthy controls, patients with UC, and patients with CPI colitis (figure 1A, online supplemental table S1). Viably cryopreserved intestinal biopsies were thawed in a single batch and digested into single-cell suspensions, which minimally impacts gene expression and cell representation in biopsies compared with fresh processing.[5] In a separate experiment, cryopreserved PBMCs from the same patients were also thawed in a single batch. For both workflows, biopsies or PBMCs were pooled in a single tube prior to processing for single-cell sequencing. After sequencing, single cells from specific patients were computationally deconvoluted by matching donor-specific single-nucleotide polymorphisms obtained from bulk RNA sequencing.[6] In a distinct workflow, a sample of thawed and digested biopsy cells was taken for separate single-cell proteomic analysis via mass cytometry (CyTOF, panel in online supplemental table S2). In total, the donors included nine patients with cancer and histoendoscopically confirmed colitis from CPI therapy: six received anti-PD-1 (αPD-1) therapy alone and three received combination αPD-1 + anti-CTLA-4 (αCTLA-4). These were compared to three healthy controls (HC) undergoing colonoscopy and three patients with UC (online supplemental table S1). One UC patient (HS6) did not yield viable single cells from biopsy after processing, but contributed to the blood data. Cells from CPI colitis patient HS11 were present in the biopsy data, but not in the blood data. Of note, most CPI colitis patients had previously received corticosteroids before biopsy, with three patients receiving TNF blockade (all had been treated with αPD-1). One individual (HS10) received vedolizumab in addition to TNF blockade for their αPD-1 colitis. While most patients had a suboptimal initial response to corticosteroids and required further immunosuppression (TNF blockade and/or vedolizumab) and were therefore steroid-refractory, three of the patients (HS7, HS8, and HS13) did eventually respond to increased corticosteroids alone (online supplemental table S1).

scRNA-seq identifies key conserved populations in CPI colitis samples

After quality control and unbiased clustering, 50,845 and 43,791 sequenced biopsy and blood cells passed filter, respectively. Using Leiden clustering followed by semi-supervised annotation (Methods, marker genes/proteins in online supplemental table S3), we identified conserved coarse immune populations in both biopsies and blood, as well as additional coarse non-immune populations in biopsies (figure 1B,C). Cells were well distributed by disease state, and prior CPI and immunosuppression (figure 1B and online supplemental figure S1). We were able to further subcluster several coarse populations (B and plasma cells, $CD4^+$ and $CD8^+$ T cells, myeloid cells, cycling populations, epithelial cells, endothelial cells, and stromal cells) into fine subpopulations in biopsies (figure 1D and online supplemental figure S2A,B) and blood (figure 1E and online supplemental figure S2C). Importantly, in colonic biopsies, this includes a cytotoxic $CD8^+$ T-cell subset expressing *GZMB*, *PRF1*, and *IFNG* ("CD8T GZMB"), a separate cytotoxic subset expressing *GZMK*, *DUSP2*, and *EOMES* ("CD8T GZMK"), as well as a distinct tissue-RM population expressing *CD69*, *ITGAE*, and *ITGA1* ("CD8T RM"). For $CD4^+$ T cells, in addition to *FOXP3*$^+$ regulatory T cells ("CD4T reg"), *CXCR5*$^+$ follicular helper T cells ("CD4T fh-like"), and *S100A4*, *VIM*, and *IL7R* expressing memory cells, there was similarly an RM population expressing *CD69*, *ITGAE*, and *ITGA1* ("CD4T RM"). Both $CD8^+$ and $CD4^+$ T cells include a naïve *KLF2*$^+$ *SELL*$^+$ subset. Hence, canonical immune and

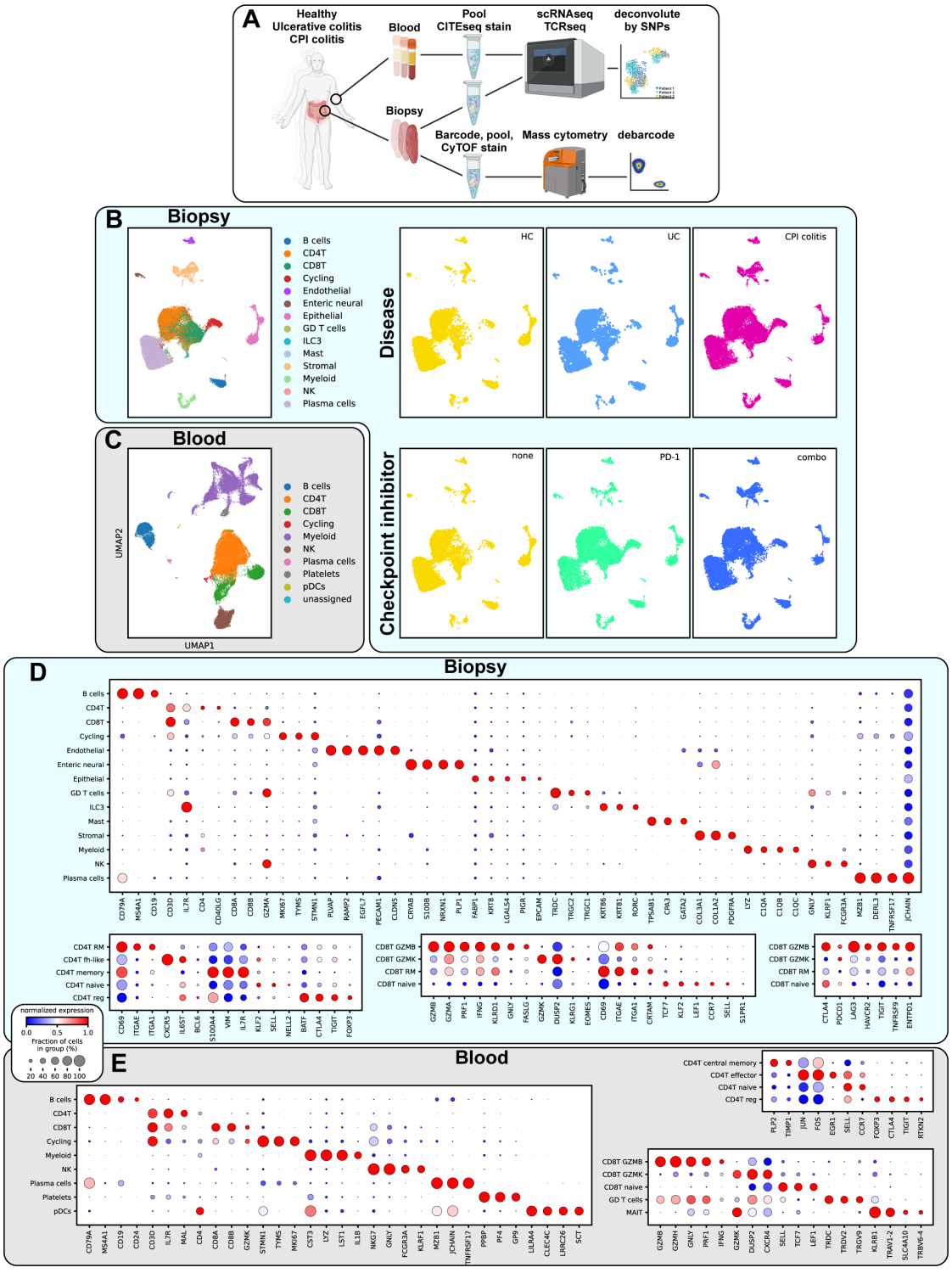

Figure 1 scRNAseq identifies key conserved populations in CPI colitis samples. (A) Schematic of study design. Peripheral blood or colon biopsies from all patients were, respectively, pooled, stained for CITE-seq, underwent scRNA-seq and TCR-seq workflows, and were later deconvoluted by patient single-nucleotide polymorphisms (SNPs) via demuxlet. A separate split of biopsy samples was barcoded, pooled, and analyzed via mass cytometry (CyTOF). (B–C) Uniform Manifold Approximation and Projection (UMAP) plots of total cells from biopsy (B) or blood (C) data. Coarse annotations are shown by color at left. Biopsy data is also separately shown by disease state and checkpoint inhibitor received. (D) Dot plots showing landmark genes for coarse annotations (top), CD4$^+$ T-cell subsets (bottom left), and CD8+T cell subsets (bottom middle) in biopsy samples. Expression of immunotherapy targets are additionally shown in CD8$^+$ T-cell subsets (bottom right). (E) Dot plots showing landmark genes for coarse annotations (left), CD4$^+$ T-cell subsets (top right), and CD8+T cell subsets (bottom right) in blood samples. CITE-seq, cellular indexing of transcriptomes and epitopes by sequencing; CPI, checkpoint inhibitors; CyTOF, cytometry by time-of-flight; HC, healthy controls; PD-1, programmed cell death protein 1; scRNA-seq, single-cell RNA sequencing; SNP, single-nucleotide polymorphisms; TCR-seq, T cell receptor sequencing; UC, ulcerative colitis.

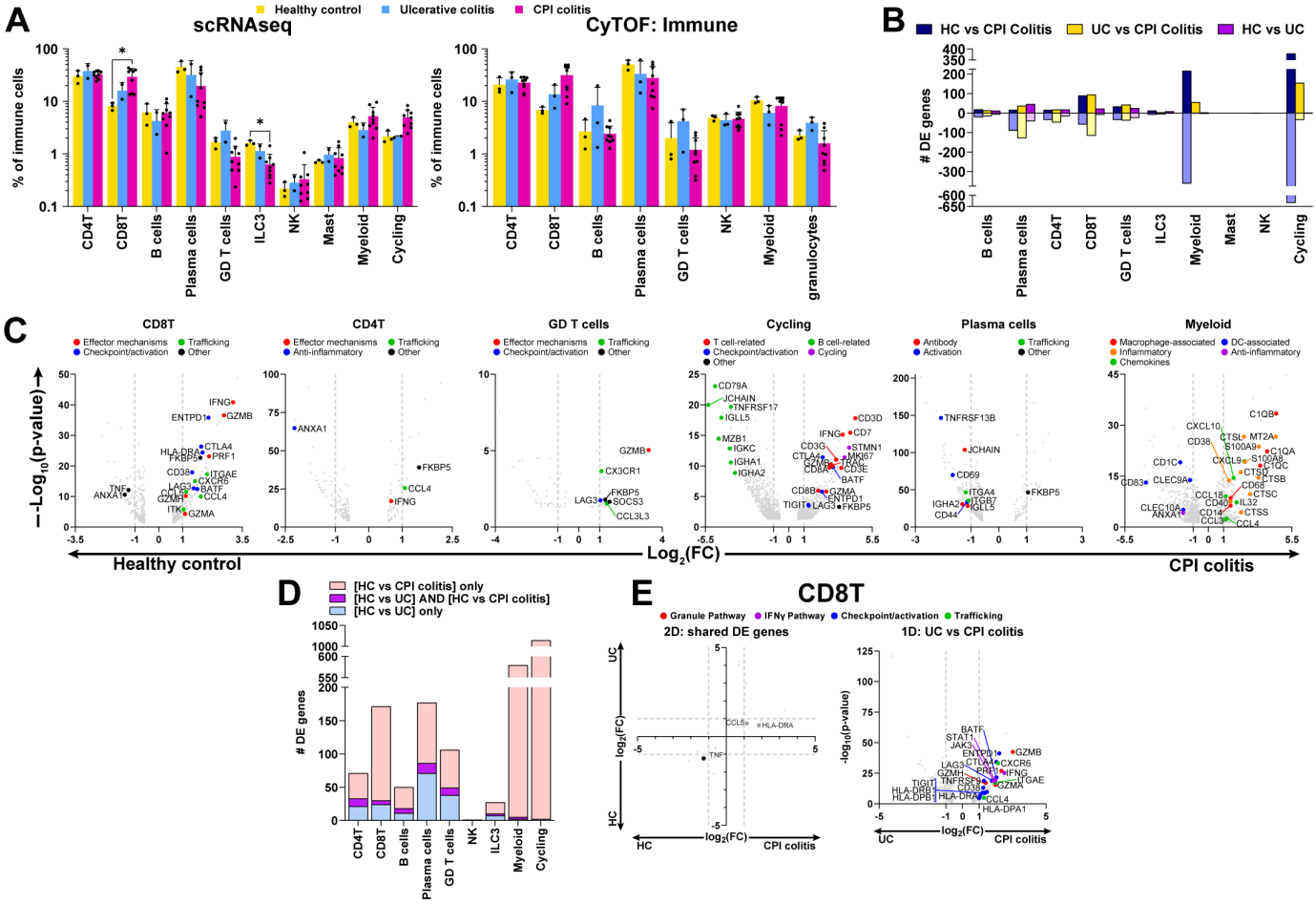

Figure 2 CPI colitis is associated with cytotoxic T-cell activity and myeloid dysregulation, distinct from ulcerative colitis. (A) Cell frequency of coarse annotated total immune cells by scRNA-seq (left) or CyTOF (right) in biopsies, stratified by disease (mean+SD; each dot represents one patient; *p<0.05 and q<0.1). (B) Number of scRNA-seq differentially-expressed (DE) genes (p<0.05 and $\log_2$(FC)>1 or <−1) between disease states, for each coarse immune population. (C) scRNA-seq DE genes in healthy versus CPI colitis biopsies by immune populations, with DE genes of interest labeled and color coded by category. (D) Number of DE genes (p<0.05 and $|\log_2(FC)| > 1$) that are found uniquely in only healthy versus CPI colitis, only healthy versus ulcerative colitis (UC), or in both comparisons in biopsy samples, for each coarse immune population. (E) Overlapping DE genes (left) in both healthy versus CPI colitis (x axis) and healthy versus UC (y axis) as well as DE genes between UC and CPI colitis (right) with genes of interest labeled, for $CD8^+$ T cells. CPI, checkpoint inhibitors; CyTOF, cytometry by time-of-flight; HC, healthy controls; scRNA-seq, single-cell RNA sequencing.

non-immune populations are identified in CPI colitis patients, including both cytotoxic and resident memory T-cell subpopulations in inflamed colitis tissues.

CPI colitis is associated with cytotoxic T-cell activity and myeloid dysregulation, distinct from ulcerative colitis

Cell abundance analysis of scRNA-seq data revealed significant enrichment of cytotoxic $CD8^+$ T cells in CPI colitis biopsies compared with HC, while group 3 innate lymphoid cells (ILC3s) were depleted (figure 2A, left). Notably, these significant changes were not seen in UC with varying endoscopic severity, compared with either CPI colitis or HC. CyTOF analysis based on manual gating of canonical cell type markers shows a similar, but not significant, trend of increased $CD8^+$ T cells in CPI colitis (figure 2A, right). In the blood, general immune subtypes did not show significant changes across disease conditions, indicating a lack of remodeling of peripheral immune responses (online supplemental figure S3C,D).

Differentially expressed gene (DEG) testing in biopsies between disease conditions further revealed large gene expression shifts ($|\log_2(\text{fold change})| > 1$) that were specific to CPI colitis tissues over both HC and UC, and occurred across multiple immune and non-immune populations (figure 2B, DEG lists by disease in online supplemental tables S4 and S5). Within the T-cell compartment, $CD8^+$ T cells upregulated numerous genes indicating an activated state, including immune checkpoints *CTLA4* and *LAG3*, ectoenzymes *ENTPD1* and *CD38*, T-cell activation marker *HLA-DRA*, and transcription factor *BATF*, which is essential for effector $CD8^+$ T-cell differentiation[7] (figure 2C). $CD8^+$ T cells also overexpressed effector molecules including *IFNG* and cytolytic genes *PRF1*, *GZMB*, *GZMA*, and *GZMH*, suggesting mechanisms for colon damage

mediated by these effector cells. Upregulation of cell trafficking-related genes including integrin *ITGAE*, chemokine receptor *CXCR6*, chemokines *CCL4* and *CCL5*, and *ITK* (which is required for gut homing[8] supports their role in T-cell recruitment to inflamed tissues. Anti-inflammatory *ANXA1* was downregulated, which has been shown to exacerbate T cell-dependent inflammation.[9] Interestingly, *TNF* was also downregulated, implying that $CD8^+$-derived TNF may not underlie inflammation in these cases of CPI colitis. Gene Set Enrichment Analysis (GSEA) confirms $CD8^+$ T-cell upregulation of pathways associated with chemokine signaling and TCR signaling including *ITK*, as well as global interferon signaling seen across cell populations (see below) (online supplemental figures S4A and S5A, online supplemental tables S6 and S7). While $CD4^+$ T cells in CPI colitis showed similar downregulation of *ANXA1* and upregulation of CCL4 and to a lesser extent *IFNG* ($\log_2$(FC)=0.68), their differential expression of other genes in CPI colitis was minimal. γδ T cells also overexpressed a similar suite of genes including *LAG3*, *GZMB*, and chemokine/receptors *CCL3L3* and *CX3CR1*. They additionally overexpressed *SOCS3*, which may provide negative feedback for interferon (IFN)-γ signaling. T cell-intrinsic gene expression changes were robust across individual patients despite distinct primary tumor types (online supplemental figure S6), arguing for a conserved adaptive immune signature in this primarily steroid-experienced CPI colitis cohort.

The cycling population is a heterogeneous population, which forms a joint cluster driven by shared overexpression of proliferative genes such as *STMN1* and *MKI67*. Because of this, we found DEGs in cycling cells in CPI colitis (over healthy) to be highly impacted by marker genes of specific constituent cell populations (figure 2C). Specifically, CPI colitis cycling populations had higher expression of cytotoxic T-cell genes including *CD3D*, *CD3G*, *CD3E*, *TRAC*, *CD7*, *CD8A*, *CD8B*, *GZMB*, *GZMA*, and *IFNG*, as well as T-cell activation markers *CTLA4*, *BATF*, *ENTPD1*, *TIGIT*, and *LAG3*, suggesting a propensity for cytotoxic $CD8^+$ T-cell subsets to proliferate in this disease state. Conversely, plasma cell-associated marker genes *CD79A*, *JCHAIN*, *IGHA1*, *IGHA2*, *IGKC*, *IGLL5*, *TNFRSF17*, and *MZB1* were downregulated in the CPI colitis cycling population, suggesting quantitative depletion of cycling plasma cells. Additionally, non-cycling plasma cells had similar downregulation of *JCHAIN*, *IGHA2* and *IGLL5*, but also survival factors *TNFRSF13B* and *CD44*[10] and gut-homing integrins *ITGA4* and *ITGB7*, pointing to the possible impairment of homing, activation, and survival of plasma cells in the CPI colitis state.

Overall myeloid gene expression changes were also similarly related to the heterogeneous composition of this population. The upregulation of lineage markers for inflammatory macrophages (*CD14*, *CD68*, *C1QA*, *C1QB*, *C1QC*), and downregulation of dendritic cell marker genes (*CD1C*, *CLEC9A*, C*LEC10A*, and *CD83*) (figure 2C) may be related to quantitative chances in their abundance (see below). In addition to this, upregulation of pro-inflammatory molecules (*CD38*, *CD40*, *IL32*; chemokines *CCL3/4/18*, *CXCL9/10*; cathepsins; and inflammatory potentiators *S100A8/ 9*), and downregulation of the anti-inflammatory molecule *ANXA1*, collectively reflect the contribution of pro-inflammatory macrophages to CPI colitis pathology.

Across the immune compartment, the changes in cell type abundance seen in CPI colitis were generally not seen in UC, arguing for distinct immunopathology. This is also supported by a comparison of gene expression changes in these two pathogenic states. Most genes that are differentially expressed in CPI colitis versus HC ($|\log_2(FC)| > 1$) were not differentially expressed when UC and HC are compared (figure 2D). This is exemplified by the cytotoxic $CD8^+$ T-cell population, which generally does not co-regulate genes in common in the healthy comparisons with either CPI colitis or UC (figure 2E, left). This is also shown by direct DE testing between CPI colitis and UC, which confirms that many of the same genes in the CPI colitis comparison with HC, are distinctly upregulated in CPI colitis as distinct effector molecules from UC. These include IFN signaling molecules *IFNG*, *STAT1*, and *JAK3*; cytotoxic genes *PRF1*, *GZMB*, *GZMA*, and *GZMH*; immune checkpoints *LAG3*, *CTLA4*, and *TIGIT*; activation molecules *CD38*, *TNFRSF9*, *BATF*, and *HLA-DRA*; and trafficking-related genes *CXCR6*, *ITGAE*, and *CCL4* (figure 2E, right). The immune checkpoints *TIGIT* and *TNFRSF9* are uniquely upregulated in the direct CPI colitis versus UC comparison (and not vs HC), pointing to unique overexpression of these regulatory mechanisms in the CPI colitis disease state. Although the UC sample size was small (n=2 with multiplexed biopsy data), and heterogenous with regard to endoscopic activity (Discussion), a separate dedicated analysis of UC patients compared with HC[5] confirmed the unique immunopathology of CPI colitis highlighted here.

The CPI colitis microenvironment is characterized by dendritic cell and macrophage dysregulation, and expanded $CD4^+$ RM precursors that are clonally related to $CD8^+$ RM and pathogenic cytotoxic T cells

Subclustering of immune populations from biopsies reveals key contributions for myeloid and T-cell subtypes. Myeloid subclustering (online supplemental figure S2A) demonstrated significant macrophage enrichment, accompanied by depletion of conventional type 1 dendritic cells (cDC1s) (figure 3A). At the level of gene expression, cDC1 cells do not show significant DEG (data not shown), but cDC2s show distinct upregulation of major histocompatibility complex (MHC) class I antigen presentation (*HLA-A, HLA-C, TAP1*), IFN induced chemokine signaling (*CXCL10*), and DC licensing/activation (*CD40*) (figure 3B, DEG lists in online supplemental table S8). They also downregulate *IL1B* which may be compensatory (figure 3B). DE programs in cDC2 were conserved across individual patients regardless of primary tumor type (figure 3C). Macrophages upregulate cathepsin C (*CTSC*) which may contribute to inflammatory pathogenesis

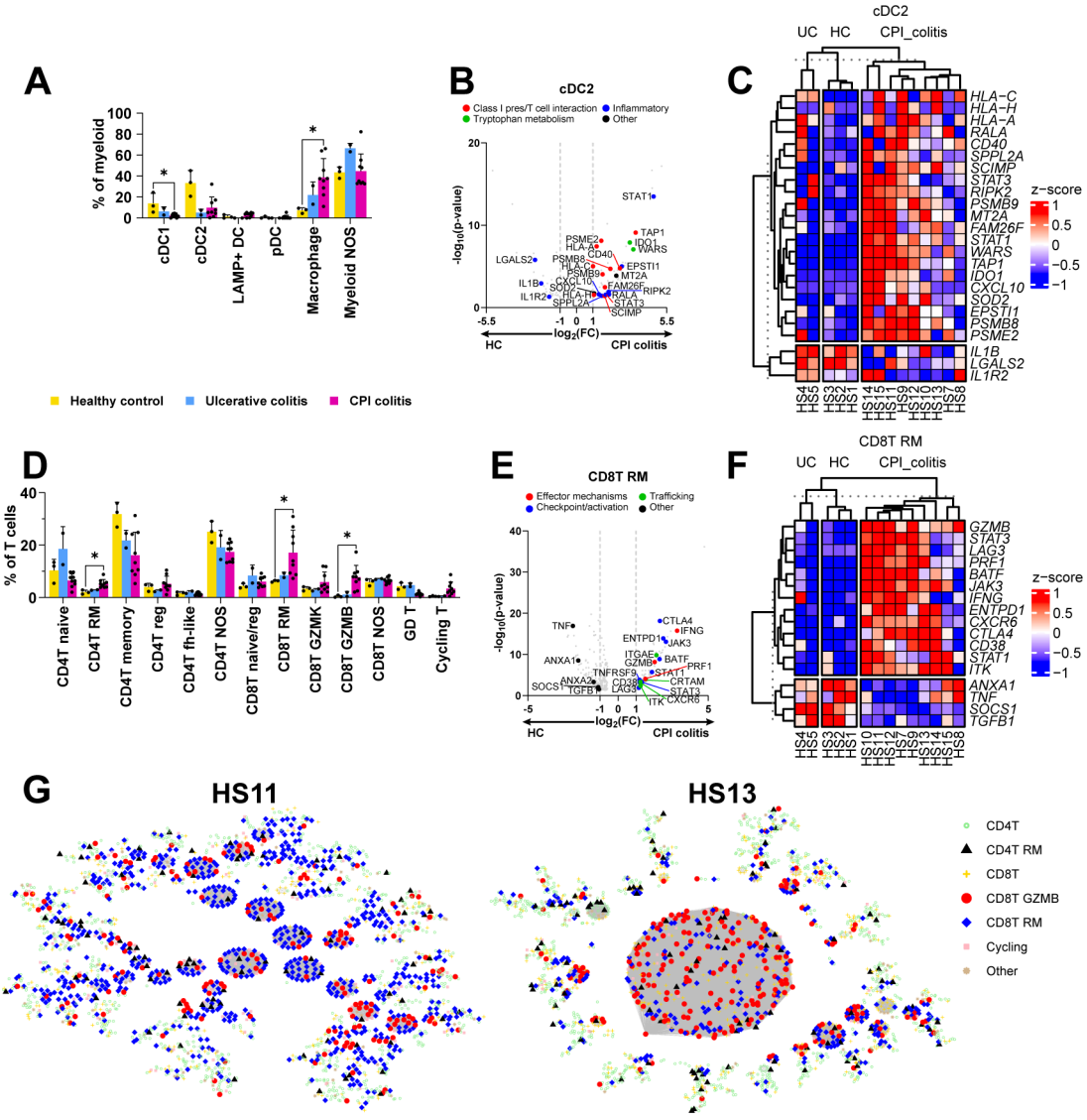

Figure 3 The CPI colitis microenvironment is characterized by dendritic cell and macrophage dysregulation, and expanded CD4$^+$ RM precursors that are clonally related to CD8$^+$ RM and pathogenic cytotoxic T cells. (A) scRNA-seq-defined myeloid subpopulation frequencies in biopsies across disease states (mean+SD; each dot represents one patient; *p<0.05 and q<0.1). (B) scRNA-seq DE genes (p<0.05 and $\log_2$(FC)>1 or <−1) in cDC2 between healthy and CPI colitis, with select genes of interest labeled. (C) Heatmap showing DE genes from (B) for cDC2 as z-scores across individual patients (columns). (D) scRNA-seq-defined T-cell subtype frequencies in biopsies across disease states (mean+SD; formatted as in A). (E) DE genes in CD8$^+$ RM cells between healthy and CPI colitis, with select genes of interest labeled. (F) Heatmap of DE genes from (E) for CD8$^+$ RM across individual patients. (G) TCR network plots for two patients with CPI colitis (HS11, HS13). Single cells with RNA and TCR data are denoted by nodes with symbols encoding their functional annotation, and cells with a common TCRαβ CDR3 sequence are grouped together in a single cluster (shaded gray circles). Nodes from biopsy data are shown. cDC1, conventional type 1 dendritic cells; LAMP, lysosomal associated membrane protein; pDC, plasmacytoid DC; myeloid NOS, myeloid not otherwise specified; CPI, checkpoint inhibitors; DC, dendritic cell; DE, differential expressed; HC, healthy controls; RM, resident memory; scRNA-seq, single-cell RNA sequencing; TCR, T cell receptor; UC, ulcerative colitis.

(data not shown). Other myeloid subpopulations did not demonstrate significant DEG (data not shown). Myeloid subpopulations in the blood (classical and non-classical monocytes, and cDCs, online supplemental figure S2C) are not detectably different in frequency in CPI colitis (online supplemental figure S3D, right).

For the T-cell subcompartment, RM precursors and cytotoxic effector populations were strongly implicated in CPI colitis. Specifically, both CD4$^+$ RM and CD8$^+$ RM populations, as well as CD8$^+$ GZMB$^+$ cells, were all significantly enriched in CPI colitis versus HC (figure 3D). CD8$^+$ GZMB$^+$ cells in particular were more than 10-fold more abundant. Cycling T cells also trended towards enrichment in CPI colitis, supporting findings from coarse DE testing of the cycling population, although this was not significant (online supplemental figure S3A, left). In addition, the CD8$^+$ RM population demonstrated dynamic regulation of gene modules in CPI colitis that

may contribute to pathogenesis, including downregulation of anti-inflammatory genes *ANXA1*, *ANXA2*, *SOCS1*, and *TGFB1* as well as an upregulation of homing and trafficking molecules *ITGAE* and *CXCR6*; immune checkpoints *CTLA4*, *LAG3*, and *ENTPD1*; activation molecules *TNFRSF9*, *CD38*, *BATF*, *JAK3*, *STAT1*, and *STAT3*; and signaling and effector molecules such as *ITK*, *CRTAM*, *PRF1*, *GZMB*, and *IFNG* (figure 3E). These findings were consistent across individual patients (figure 3F). GSEA for $CD8^+$ RM underscores the upregulation of adaptive immune signaling via *ITK*, *CTLA4*, *LAG3*; cytokine signaling via *JAK3* and *STAT1*; and downregulation of interleukin signaling supported by *ANXA1*, *TGFB1*, *TNF*, and *SOCS1* (online supplemental figure S4C and S5C, online supplemental tables S6 and S7). $CD4^+$ RM and $CD8^+$ GZMB populations demonstrated few to no DEGs in CPI colitis. However, cytotoxic $CD8^+$ GZMB cells compared with their RM counterparts express higher levels of cytolytic genes (*GZMB*, *NKG7*, *PRF1*, *GNLY*, *GZMA*, *GZMH*), effector molecules (*IFNG*), and chemokines (*CCL3*, *CCL4*), which would be consistent with their role as effector cells causing terminal epithelial damage (data not shown). Generally significant changes by frequency were not seen in other immune subpopulations (cycling, B, plasma cells) in biopsies (online supplemental figure S3A), or T-cell subpopulations in the periphery (online supplemental figure S3D, right).

Clonal analysis of these specific T-cell phenotypes implicates developmental relationships between both RM populations and terminal $GZMB^+$ effectors. We obtained paired TCR data from single cells with transcriptome data (biopsies: 15,394 cells with TCRβ and 12,810 cells with TCRαβ paired with RNA data; blood: 17,694 cells with TCRβ and 12,714 cells with TCRαβ paired with RNA data). We used the NAIR analytic approach[11] to identify expanded clusters of single cells where >1 cell shared the same TCRαβ heterodimer. This revealed that biopsies from CPI colitis patients had significantly higher numbers of expanded clusters (normalized to the total number of cells per sample) compared with both HC and UC (online supplemental figure S7A). Consistent with this finding, total T cells from CPI colitis biopsies had a significantly higher Gini coefficient (0.18) than HC (0.07, p=0.013), which was also numerically higher than UC although not significant (0.14, p=0.099), consistent with clonal expansion in the CPI colitis state (online supplemental figure S7B). T cells from the blood of these patients did not demonstrate significant changes in the numbers of expanded clusters or Gini coefficient in CPI colitis, consistent with minimal remodeling of the overall peripheral T-cell repertoire (online supplemental figure S7A,B). Moreover, network analysis indicates increased TCRαβ clonotype sharing between RM and cytotoxic phenotypes in CPI colitis. Looking at expanded clusters in biopsies, although HC tissue has low-level pairwise sharing between $CD4^+$ RM, $CD8^+$ RM, or $CD8^+$ GZMB populations (range: 1.3–2.5% of expanded clusters), all of these frequencies are increased in CPI colitis (range: 8.8–22% of expanded clusters). In addition, individual clusters in CPI colitis biopsies exhibit three-way sharing between all three populations (7.2% of expanded clusters), which is never seen in HC (single patient network plots in figure 3G, quantitation in online supplemental figure S7C,D). The clonotype sharing, which is the result of irreversible somatic rearrangement of the CDR3 locus, indicates a direct developmental relationship between these populations. Furthermore, given the known role of RM cells in rapid tissue responses to previously encountered antigens, and the higher cytolytic effector program of the $GZMB^+$ cells, this supports a model where both $CD4^+$ RM and $CD8^+$ RM cells act as directly related tissue precursors, which on recognition of tissue antigens give rise to $CD8^+$ GZMB progeny responsible for tissue damage in CPI colitis.

Stromal and endothelial cells in CPI colitis uniquely dysregulate NAD^+ and tryptophan metabolism, while both CPI colitis and UC converge on loss of epithelial homeostasis

In the non-immune compartment in CPI colitis biopsies, epithelial, endothelial, stromal and enteric neural cells do not demonstrate significant changes in abundance this disease state (figure 4A, left), which is corroborated by orthogonal CyTOF (figure 4A, right), However, significant gene expression changes are seen in all these populations in CPI colitis, relative to either UC or HC (figure 4B, DEG lists by disease in online supplemental tables S4 and S8). Specifically, the stromal and enteric neural populations share upregulation of neutrophil chemokines (*CXCL1/7/8/9/10*), proinflammatory *IL32*, as well as possible compensatory mechanisms such as *IL18BP* (which inhibits IL18 signaling) and metallothioneins that scavenge reactive oxygen species (figure 4C). While generally these changes are conserved across the majority of individual CPI colitis patients, several patients (HS8, HS10, HS13) represent a subset that upregulate these programs to a lesser degree (online supplemental figure S6). This may be related to their lower endoscopic severity score (0–1), or for patients HS8 and HS13, the fact that they responded to increased corticosteroids alone (online supplemental table S1), but this will require further study and validation.

Interestingly, GSEA analysis for stromal cells in CPI colitis versus HC not only supports upregulation of proinflammatory cytokine signaling and metallothioneins, but also identifies changes in metabolism, specifically a common focus on increased NAD^+ catabolism (*NAMPT*, *NNMT*), as well as tryptophan metabolism (*WARS*, *IDO1*) (online supplemental figures S4B and S5B and online supplemental tables S6 and S7 for GSEA, figure 4C for volcano plots of individual genes). These same metabolic genes are also significantly upregulated in enteric neural cells from CPI colitis versus HC (figure 4C). While these pathways have been implicated in UC pathogenesis,[12 13] they also distinctly characterize stromal cells in CPI colitis. Most DE genes between CPI colitis versus HC are distinct from genes from UC comparisons to healthy (figure 4D,E,

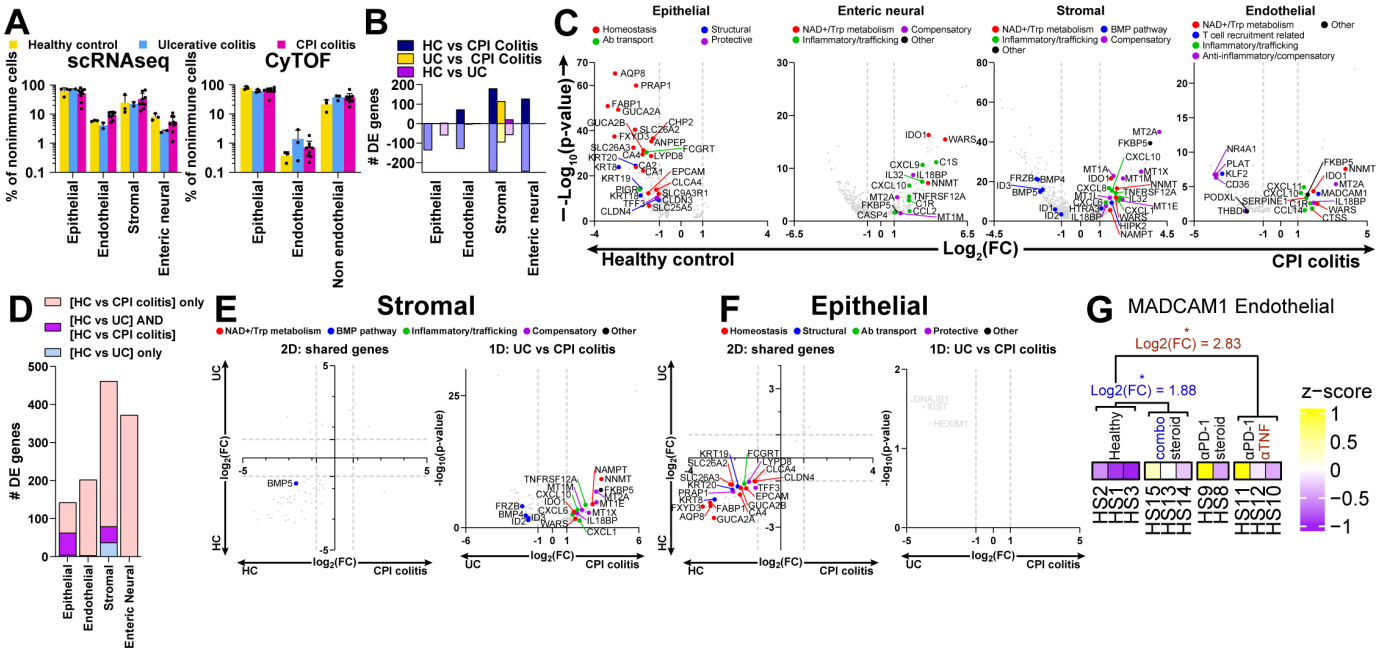

Figure 4 Stromal and endothelial cells in CPI colitis uniquely dysregulate NAD$^+$ and tryptophan metabolism, while both CPI colitis and UC converge on loss of epithelial homeostasis. (A) Cell frequency of coarse-annotated total non-immune cells by scRNA-seq (left) or CyTOF (right) in biopsies, stratified by disease states (mean+SD; each dot represents one patient; *q<0.1). (B) Number of scRNA-seq differentially-expressed (DE) genes (p<0.05 and $\log_2$(FC)>1 or <−1) between disease states, for each non-immune population. (C) DE genes in healthy versus CPI colitis biopsies by non-immune populations, with DE genes of interest labeled. (D) Number of DE genes (p<0.05 and $|\log_2(FC)| > 1$) that are found uniquely in either healthy versus CPI colitis, healthy versus ulcerative colitis (UC), or both comparisons in biopsy samples, for each non-immune population. (E–F) Overlapping DE genes (left) in both healthy versus CPI colitis (x axis) and healthy versus UC (y axis) as well as DE genes between UC and CPI colitis (right) with genes of interest labeled, for stromal cells (E) and epithelial cells (F). (G) Heatmap showing relative expression (z-score) of *MADCAM1* in endothelial cells for individual patients (healthy controls, or patients with CPI colitis with distinct CPI exposure and immunosuppression). Fold change reported for comparisons with significant changes (p<0.05) relative to healthy controls (HS1-3). CPI, checkpoint inhibitors; CyTOF, cytometry by time-of-flight; HC, healthy controls; scRNA-seq, single-cell RNA sequencing.

left), and in direct comparisons between UC and CPI colitis, NAD$^+$ catabolism, tryptophan metabolism, and metallothionein genes are again uniquely upregulated in CPI colitis stroma (figure 4E, right). Stromal handling of NAD$^+$/tryptophan may therefore be unique to CPI colitis over other colitis states, via diminished epithelial survival via NAD$^+$ depletion, increased toll-like receptor 2 and 4 activation by WARS,[14 15] or compensatory inhibition of inflammation via IDO-mediated tryptophan depletion.

We also observe CPI colitis-specific dysregulation of the BMP pathway in stromal cells, which is a known contributor to colitis models as it modulates intestine morphogenesis, homeostasis, and inflammation.[16] Specifically, we see downregulation of the Wnt regulator *BMP4*, which is anti-inflammatory and protective in DSS-induced colitis models through stem cell maintenance and epithelial proliferation, along with its downstream targets *ID/1/2/3*.[16–18] Furthermore, we also see downregulation of Wnt antagonist *FRZB*, and BMP4 antagonists *HIPK2* and *HITRA3*[19–21] (figure 4C,E). Despite some heterogeneity in upregulated gene modules in stromal cells across patients, the downregulation of BMP and Wnt signaling is highly conserved across individuals (online supplemental figure S6). GSEA analysis points to possible effects of BMP4 downregulation on IGF transport and elastic fiber formation as well (online supplemental figure S5B and online supplemental tables S6 and S7). Together, these results suggest decreased BMP activity in CPI colitis, which could further exacerbate colonic damage and inflammation.

While epithelial cells also have substantial gene expression changes in CPI colitis (figure 4B,D), these may represent a shared program of epithelial loss of homeostasis across colitis states. Specifically, epithelial cells in CPI colitis (over healthy) showed downregulation of many homeostatic genes (*GUCA2A*, *GUCA2B*, *CHP2*, *ANPEP*), small molecule transporters (*AQP8*, *SLC25A5*, *SLC26A2*, *SLC26A3*, *SLC9A3R1*, *CLCA4*, *FXYD3*, *FABP1*, *CA1*, *CA2*, *CA4*), and protective molecules (*TFF3*, *PRAP1*, and *LYPD8*) (figure 4C). Epithelial cells also downregulated genes related to structure (*EPCAM, KRT8/18/19/20*, *CLDN3/4*), and antibody transport function (*PIGR*, *FCGRT*). These downregulated genes are highly conserved across individual patients (online supplemental figure S6). Of note, almost half the DEGs between HC versus CPI colitis, and nearly all DEGs between HC versus UC, consisted of shared dysregulated genes (figure 4F, left), while there were almost no DEGs between CPI colitis

and UC (figure 4F, right). Shared genes downregulated in both UC and CPI colitis were many of the aforementioned genes also downregulated compared with healthy that are involved in homeostasis, transport, and structure (figure 4F, left). Together these results indicate that although UC and CPI colitis may have distinct immune mechanisms, both pathologic states converge on loss of intestinal homeostasis modules.

Endothelial cells in CPI colitis upregulate MAdCAM-1, the ligand of integrin α4β7, particularly after TNF blockade and αCTLA-4

Endothelial cells in CPI colitis contribute to pathogenesis in several respects. In addition to their overexpression of chemokines promoting inflammation (eg, *CCL14, CXCL11*), and downregulation of *KLF2* which inhibits T-cell rolling and adhesion to endothelium[22] (figure 4C, DEG lists by disease in online supplemental table S4), the CPI colitis endothelial cells significantly upregulated *MADCAM1*, the ligand for integrin α4β7. α4β7 binding to *MADCAM1* facilitates T-cell recruitment to the gut.[23 24] Vedolizumab is a monoclonal antibody against α4β7, that is, Food and Drug Administration approved for both Crohn's disease and UC, and it is frequently used off-label for CPI colitis.[25] However, the specific CPI colitis disease states that may be more responsive to this therapy are unknown. In an exploratory analysis, *MADCAM1* was particularly upregulated in patients who received prior TNF blockade, as well as those who received a combination of αCTLA-4 with αPD-1 CPI (figure 4G, DEG lists by suppression in online supplemental table S9). While this analysis is limited by sample size and heterogeneity, these findings suggest that patients with αCTLA-4-induced colitis, or those who do not respond to steroids or anti-TNF therapy, may benefit from vedolizumab.

CPI colitis features global IFN-γ response including enhanced antigen presentation

To gain a broader look at other pathways in CPI colitis, we looked at genes that were commonly overexpressed across multiple coarse populations compared with HC. Interestingly, of the top fifteen genes that were upregulated in the greatest number of populations, 12 emerged

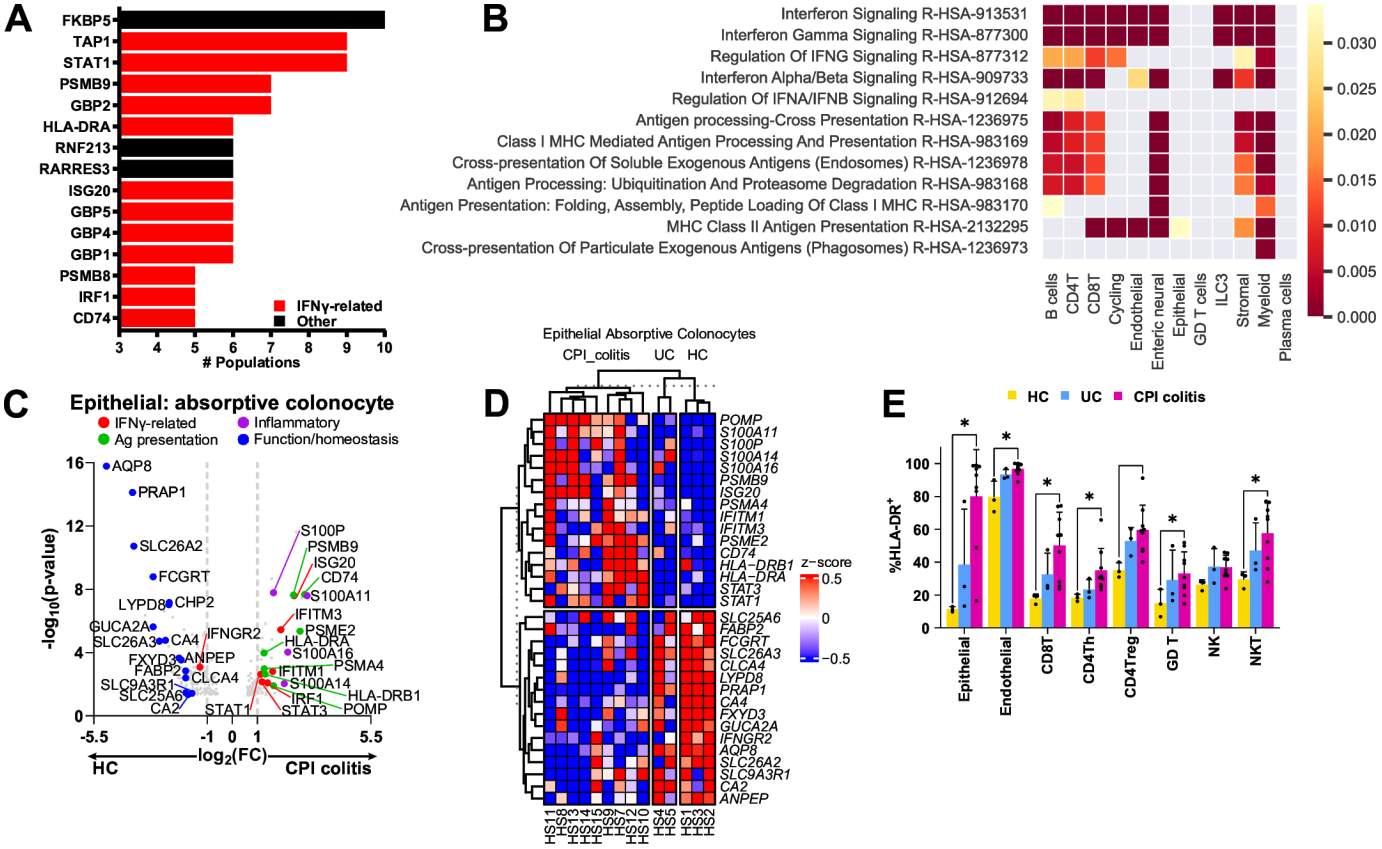

Figure 5 CPI colitis features global IFN-γ response including enhanced antigen presentation. (A) Single-cell RNA sequencing genes upregulated across the greatest number of coarse populations ($p<0.05$ and $\log_2(FC)>1$) in healthy versus CPI colitis. (B) Gene Set Enrichment Analysis showing significantly upregulated pathways (rows) across coarse cell populations (columns) relating to either interferon signaling (top rows) or antigen presentation (bottom rows). (C) DE genes between healthy and CPI colitis biopsies in epithelial absorptive colonocytes. Genes of interest are labeled. (D) Heatmap showing DE genes from (C) across individual patients. (E) Protein expression of HLA-DR by CyTOF in non-professional antigen-presenting populations (mean+SD; each dot represents one patient; *$p<0.05$ and $q<0.1$). CPI, checkpoint inhibitors; CyTOF, cytometry by time-of-flight; DE, differentially expressed; HC, healthy controls; IFN, interferon; MHC, major histocompatibility complex; UC, ulcerative colitis.

as downstream of IFN signaling (figure 5A, DEG by disease in online supplemental table S4). This included IFN-γ signaling molecule *STAT1*, early IFN-γ response genes *GBP1*, *GBP2*, *GBP4*, *GBP5*, *ISG20*, and *IRF1*, and, interestingly, antigen presentation-related genes *HLA-DRA*, *CD74*, *TAP1*, and immunoproteasome subunits *PSMB8* and *PSMB9*. Of note, the most frequently overexpressed gene was *FKBP5*, which associates with and regulates the steroid receptor complex and trafficking[26] and may be compensatory in this predominantly steroid-experienced setting. Looking closer at each population, we found many immune and non-immune cell types upregulating molecules in CPI colitis related to IFN-γ-JAK-STAT signaling (*IFNGR2*, *JAK2*, *STAT1/3*) and gene modules expressed in response to IFN-γ (*GBP**, *IFITM**, *IRF**) (GSEA results in figure 5B and online supplemental tables S6 and S7, DE genes in online supplemental figure S8A). Overexpression of IFNG only in $CD8^+$ (eightfold enriched), cycling, and $CD4^+$ populations implicates T cells as the primary source for IFN-mediated effects.

Additionally, antigen presentation modules were also upregulated globally, in both professional and non-professional antigen-presenting immune and non-immune cells, which may occur in response to IFN-γ signaling (GSEA results in figure 5B and online supplemental tables S6 and S7). These include both HLA class I and II genes, *TAP1*, *CD74*, *CIITA*, as well as proteasome subunit genes and immunoproteasome subunits (*PSMB8/9/10*) (DE genes in online supplemental figure S8B).

Interestingly, among the epithelial subpopulations, the absorptive colonocyte may specifically integrate homeostasis and IFN-mediated inflammation. This is because this population appears to be a target for tissue damage—absorptive colonocytes were significantly depleted in CPI colitis (online supplemental figure S3B, left), even when the total epithelial population was not (figure 4A). In addition, these absorptive colonocytes downregulated many of the previously mentioned homeostatic genes (figure 5C) seen in coarse epithelial comparisons (figure 4C), but distinct from coarse epithelial cells, these colonocytes exhibited unique overexpression of IFN-γ signaling (*STAT1/3*, *IFITM1/3*, *ISG20*), downstream antigen presentation (*HLA-DRA/B1*, *CD74*, *PSMA4*, *PSMB9, PSME2*), as well as inflammatory genes (*S100P*, *S100A11/14/16*) and *POMP*, a chaperone protein required for assembly of both the proteasome and immunoproteasome (figure 5C, DEG lists by disease in online supplemental table S8). Colonocyte gene expression changes were highly conserved across individuals (figure 5D). Pathway analysis supports upregulation of inflammatory pathways, as well as downregulation of metabolic and small molecule transport pathways as indicated by decreased *SLC**, *AQP**, and *ATP* transcript expression (online supplemental figure S4C and S5C). Together, these signatures additionally implicated absorptive colonocytes as the epithelial convergence point of IFN-γ-induced signaling, antigen presentation, and inflammation.

We confirmed this trend of increased antigen presentation by looking at HLA-DR expression in non-professional antigen-presenting cells by CyTOF (figure 5E). Epithelial, endothelial, $CD8^+$ and $CD4^+$ T cells, $CD4^+$ T regulatory (Treg) cells, and natural killer T (NKT) cells all significantly upregulated HLA-DR in CPI colitis. The effect was especially striking in both epithelial cells and $CD8^+$ T cells, going from almost no HLA-DR expression in both populations in HC tissue to an average of 60% and 20% $HLA\text{-}DR^+$ epithelial and $CD8^+$ T cells, respectively. While HLA-DR can be an activation marker in human T cells, its upregulation (along with IFN-inducible proteasome subunits) across cell types suggests that IFN signaling in inflamed CPI colitis tissues may establish a feedback loop leading to upregulated antigen presentation, including a possible presentation by non-professional antigen presenting cells (APCs). This enhanced antigen presentation, including altered peptide isoforms generated by immunoproteasome subunits, may potentially drive CPI colitis pathogenesis.

Unbiased CyTOF clustering reveals activated $HLA\text{-}DR^+$ $CD38^+$ cytotoxic $CD8^+$ and $CD4^+$ RM populations

Because our transcriptomic data suggested that $CD8^+$ T-cell activation was pivotal to CPI colitis pathology, we looked at activation markers expressed by $CD8^+$ T cells via CyTOF for proteomic confirmation. CPI colitis $CD8^+$ T expressed significantly more $CD38^+$ cells and less $CD27^+$ compared with HC (figure 6A). Additionally, we observed trends (not significant) of increased $CTLA\text{-}4^+$ and T cell immunoreceptor with immunoglobulin and ITIM domains $(TIGIT)^+$ populations. Of note, we saw no trends in PD-1 expression by both RNA and protein.

Separately, we additionally performed unbiased clustering and visualized our CyTOF data via Uniform Manifold Approximation and Projection (UMAP) (Cyclone[27]) to investigate unanticipated cell populations. This identified several populations that clustered based on HLA-DR expression (figure 6B,C). Several epithelial cellular adhesion molecule $(EpCAM)^+$ epithelial clusters emerged, that also expressed HLA-DR. Interestingly, $CD3^+$ T cells ($CD4^+$, $CD8^+$, and $CD4^-CD8^-$ T (dnT)) were split into respective clusters that either co-expressed $HLA\text{-}DR^+CD38^+$ or did not ($HLA\text{-}DR^-CD38^-$). Both surface markers have been shown to mark activated T cells, in particular, HLA-DR, and their co-expression identified a distinct activated T-cell subset in the CPI colitis microenvironment using unsupervised analysis.

Looking at cell population frequencies in the unbiased CyTOF clusters, we found a significant increase in $HLA\text{-}DR^+$ accompanied by a significant decrease in $HLA\text{-}DR^-$ epithelial cell frequencies in CPI colitis compared with healthy (figure 6D). Additionally, all three ($CD4^+$, $CD8^+$, dnT) $HLA\text{-}DR^+CD38^+$ T-cell clusters showed a trend towards increased frequency which was not statistically significant. Because our unbiased clustering revealed a strong correlation between HLA-DR and CD38 expression in T cells, we also manually applied this co-expression

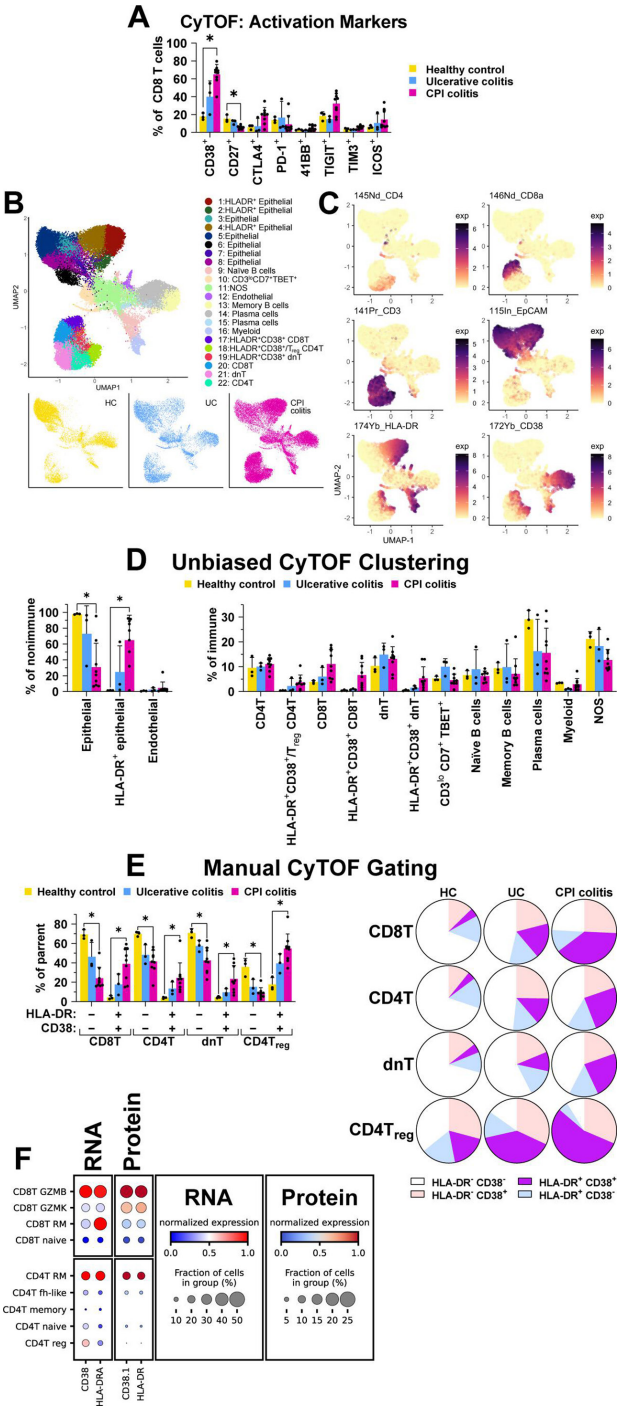

Figure 6 Unbiased discovery reveals activated HLA-DR$^+$ CD38$^+$ cytotoxic CD8$^+$ and CD4$^+$ RM populations. (A) Protein expression by unbiased CyTOF analysis of T-cell checkpoint/activation markers in CPI colitis biopsies, stratified by disease states (mean+SD; each dot represents one patient; *p<0.05 and q<0.1). (B) CyTOF UMAP plots of all live-cell events, color-coded by annotated unbiased clusters. Data is also shown separately in the inset below by disease state. (C) Feature plots of select marker expression projected on the UMAP space from (B) specifically CD4, CD8a, CD3 for T cells; EpCAM for epithelial cells; HLA-DR for class II antigen presentation and activated T cells; CD38 for activated T cells. (D) Non-immune (left) and immune (right) population frequencies based on unbiased clustering of CyTOF data, by disease state (formatted as in A). (E) CyTOF expression of manually gated HLA-DR and CD38 in T-cell subsets, by disease state. (Bar graph: formatted as in A); pie chart: per cent of each population shown). (F) scRNA-seq (RNA) and CITE-seq (protein) expression of CD38 and HLA-DR(A) in scRNA-seq defined T subpopulations. CITE-seq, cellular indexing of transcriptomes and epitopes by sequencing; CPI, checkpoint inhibitors; CTLA-4, cytotoxic T-lymphocyte-associated antigen 4; CyTOF, cytometry by time-of-flight; EpCAM, epithelial cell adhesion molecule; HC, healthy controls; PD-1, programmed cell death protein 1; RM, resident memory; scRNA-seq, single-cell RNA sequencing; UC, ulcerative colitis; UMAP, Uniform Manifold Approximation and Projection; TIM3, T-cell immunoglobulin and mucin-domain containing 3; TIGIT, T cell immunoreceptor with immunoglobulin and ITIM domains; ICOS, inducible T cell costimulator.

gate to our CyTOF T-cell populations. In $CD8^+$ T $CD4^+$ T, dnT, and $CD4^+$ Treg cells, there was a significant increase in manually gated $HLA\text{-}DR^+CD38^+$ populations, accompanied by a significant decrease in $HLA\text{-}DR^-CD38^-$ cells in CPI colitis (figure 6E).

Lastly, we also looked at HLA-DR and CD38 expression in our scRNA-seq object, on the transcript and protein (CITE-seq) level to understand what T-cell subpopulation are marked by co-expression of these markers. By both RNA and protein, two of the populations that are quantitively enriched in CPI colitis ($CD8^+$ GZMB and $CD4^+$ RM cells, figure 3D) were positive for both HLA-DR and CD38, indicating that their specific activation is linked to the CPI colitis state (figure 6F). The third T-cell population that was enriched in CPI colitis ($CD8^+$ RM cells) was strongly positive for *HLA-DRA* transcript but not *CD38*. Overall, HLA-DR and CD38 co-expression may mark the pathologically relevant, activated T cells in CPI colitis, which includes $CD4^+$ RM precursors as well as $CD8^+$ cytotoxic effectors, narrowing the target cells for potential therapeutic strategies.

CPI colitis from αPD-1 and combination αPD-1/αCTLA-4 have distinct immunopathological features

We also investigated the distinct mechanisms of colitis induced by αPD-1 versus combination αPD-1/αCTLA-4 treatment. Exploratory comparisons were restricted to the two patients with αPD-1 colitis who received only steroids (HS8 and HS9), versus the three patients with αPD-1/αCTLA-4 colitis who also received only steroids (HS13, HS14, HS15), to ensure consistent immunosuppression for comparability. The myeloid population demonstrates more gene expression changes with combination blockade (figure 7A, top; online supplemental table S10). Many combination-upregulated genes related to monocytes/macrophages (*CD14, S100A8/9*), chemotaxis and trafficking (integrin *ITGB2*, *CCL4, CXCL2/3*, complement receptors *C3AR1/C5AR1*), inflammatory signaling (*IL1R2, IFNGR2*, *TLR2*), and compensatory anti-inflammatory signaling (metallothioneins). Conversely, αPD-1 colitis demonstrated upregulation of *ITGB7* and *CLEC10A* (figure 7B, top left). Many of the inflammatory/myeloid genes upregulated in combination colitis were also upregulated in αPD-1 colitis but to a lesser extent compared with healthy (figure 7B, top right). However, overall myeloid composition was not significantly different between CPI (figure 7C, top).

Distinct differences were also seen in the CD8T compartment, where both αPD-1 and combination colitis induced robust differential expression versus HC (figure 7A, bottom; online supplemental table S10). While combination colitis showed a propensity for integrin *ITGB2* and granzyme K (*GZMK*), as previously described,[3] these patients also upregulated co-stimulation (*ICOS*) and other immune checkpoints including *ENTPD1* and *CD27*. αPD-1 colitis involved a distinct program with upregulation of cytotoxic genes (*NKG7, GNLY, GZMM, CRTAM*), distinct integrins (*ITGAE, ITGB7*), and multiple MHC class II isoforms indicative of T-cell activation (figure 7B, bottom left). This αPD-1 associated cytotoxic program was also upregulated in combination colitis versus healthy, although to a lesser extent (figure 7B, bottom right). T-cell subset frequency was not significantly different by CPI (figure 7C, bottom).

Other modules of genes were co-regulated across cell types in each form of CPI colitis. In general, IFN target genes including *IFNGR1* and *IFNGR2* were more upregulated in αCTLA-4 colitis, although unexpectedly *IFNG* upregulation itself was seen in αPD-1 colitis in cycling and enteric neural cells (figure 7D, left). MHC class I expression in plasma cells and MHC class II expression in enteric neural cells were highest in αCTLA-4 colitis, while MHC class II upregulation in CD8T and cycling populations (likely from cycling T cells) were more pronounced in αPD-1 colitis (figure 7D, right). Overall, these findings point to distinct modules of myeloid-related inflammation, co-stimulation and antigen presentation from αPD-1/αCTLA-4 colitis, versus cytotoxic signaling and T-cell activation that drives αPD-1 colitis.

External validation underscores a conserved role for activated CD4 RM T cells and cDC dysregulation in CPI colitis across the steroid exposure spectrum

To understand what features of the CPI colitis tissue microenvironment are conserved regardless of steroid exposure, we validated our findings in a recently published scRNA-seq data set of CD45-sorted immune cells from patients with steroid-naïve melanoma with endoscopically confirmed CPI colitis on biopsies, or who received CPI but had no colitis on endoscopy.[2] We adopted similar filtering and analytic workflows including annotation as we had applied to our own data (Methods, marker gene annotation online supplemental table S3). This reveals similar canonical immune types (figure 8A,B). Similar to our primarily steroid-experienced work, there was quantitative enrichment of cytotoxic CD8 T cells and macrophages, as well as depletion of cDC1, cDC2, and ILC3 cells which was not described in the original report (figure 8C). These changes in cell type frequency were only seen in CPI colitis and not merely with CPI treatment, suggesting these are shared features specific to the CPI colitis state (and not a treatment effect of CPI exposure alone), and are conserved regardless of cancer type or steroid exposure. The steroid-naïve data set does indicate more robust increases in cycling cells and depletion of plasma cells compared with our predominantly steroid-experienced samples. While CPI treatment alone does modulate many similar genes to CPI colitis, there is still a distinct gene expression program associated with the colitis state with a larger number of genes specifically upregulated in CPI colitis over CPI-treated patients without colitis (figure 8D,E, DEG lists in online supplemental table S11). Some of this program is driven by IFN signaling; as previously reported and as in our own data, the most frequently upregulated genes across populations are mostly IFN-related (figure 8F, also online supplemental

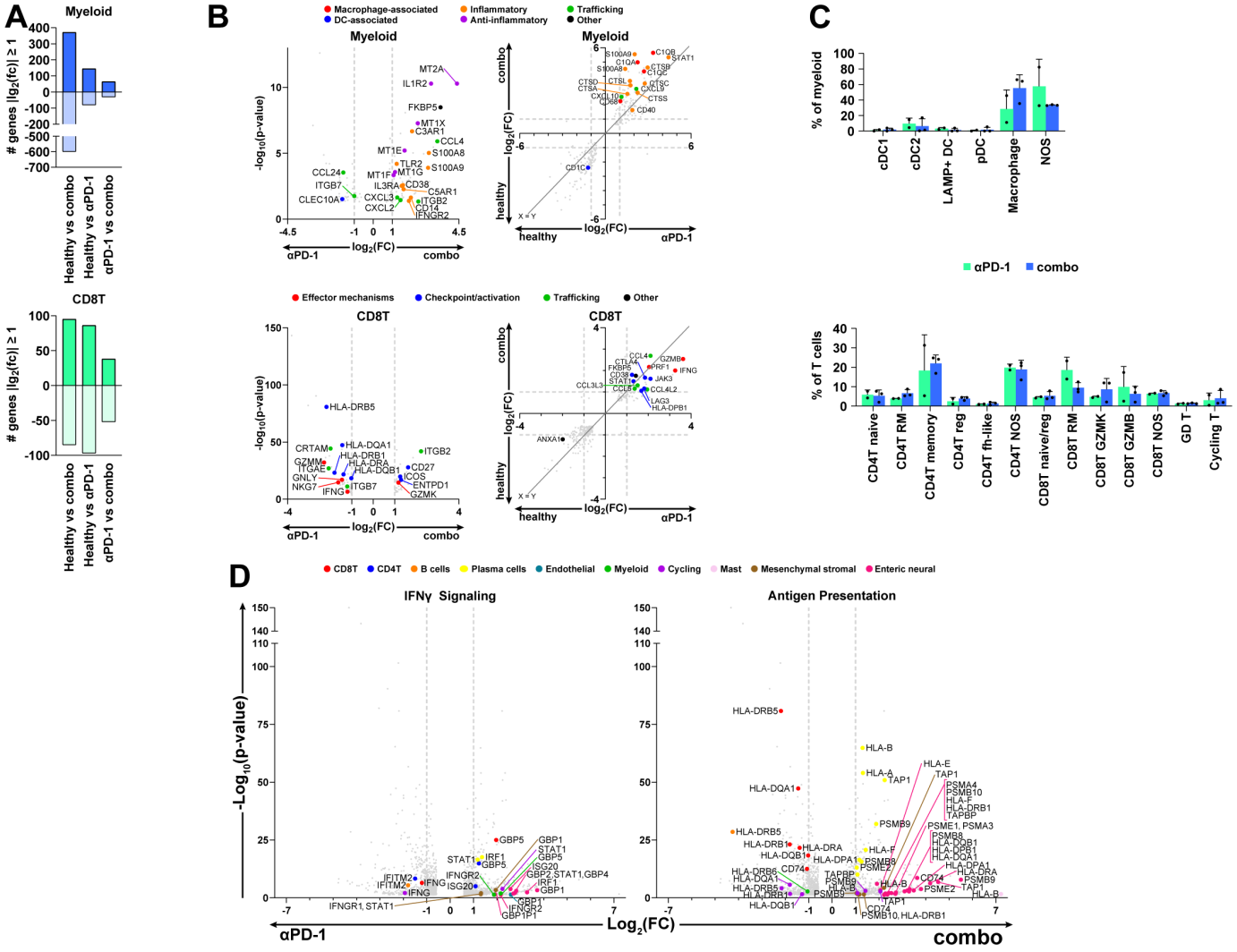

Figure 7 Checkpoint inhibitors colitis from αPD-1 and combination αPD-1/αCTLA-4 have distinct immunopathological features. (A–C) Single-cell RNA sequencing biopsy results for myeloid cells (top row), and CD8$^+$ T cells (bottom row). (A) Number of DE genes (p<0.05 and $\log_2$(FC)>1 or <−1) between healthy, αPD-1 colitis, and αPD-1 + αCTLA-4 (combo) colitis. (B) DE genes (p<0.05 and $\log_2$(FC)>1 or <−1) between αPD-1 and combo (left) and overlapping DE genes (right) in both healthy versus αPD-1 (x axis) and healthy versus combo (y axis), with genes of interest labeled. (C) Subpopulation cell frequencies in αPD-1 and combo colitis patients. (mean+SD; each dot represents one patient). (D) DE genes between αPD-1 and combo, with genes related to IFN-γ signaling (left) or antigen presentation (right) labeled. cDC1, conventional type 1 dendritic cells; CTLA-4, cytotoxic T-lymphocyte-associated antigen 4; DC, dendritic cell; DE, differentially expressed; IFN, interferon; LAMP, lysosomal associated membrane protein; NOS, not otherwise specified; PD-1, programmed cell death protein 1; pDC, plasmacytoid dendritic cell.

figure S9A), although of note, *FKBP5* is not frequently upregulated in this validation data set, consistent with its lack of induction in these steroid-naïve patients. Strikingly, many of the other co-regulated genes in both CPI treatment and CPI colitis are similar in this steroid-naïve versus our mostly steroid-experienced data (figure 8G). These include: in CD8$^+$ T cells, immune checkpoints such as *CTLA4, LAG3, HAVCR2* (as described) plus *ENTPD1* and the activation markers *HLA-DRA* and *CD38*; and in myeloid cells, inflammatory pathways such as the chemokines *CXCL9* and *CXCL10, IL1B*, and *S100A8* and *S100A9* (also as described). Intriguingly, CD8$^+$ T cells also downregulate *TNF* and anti-inflammatory *ANXA1* as in the steroid-experienced data. In cDCs, *WARS* and *IDO* are again upregulated as in our data, validating a role for tryptophan metabolism across steroid exposure states. Altogether, this external validation argues for conserved cytotoxic and myeloid inflammatory states driven by IFN signaling between steroid-naïve and our predominantly steroid-experienced CPI colitis across cancer patients (many of whom are steroid-refractory), and also validates cDC/ILC3 depletion and altered tryptophan metabolism from our data as additional conserved CPI colitis hallmarks.

Identification of T-cell subsets based on subclustering (marker genes for annotation in online supplemental table S3) identifies similar tissue populations including cytotoxic, cycling, gd, and MAIT cells (figure 8H,I).

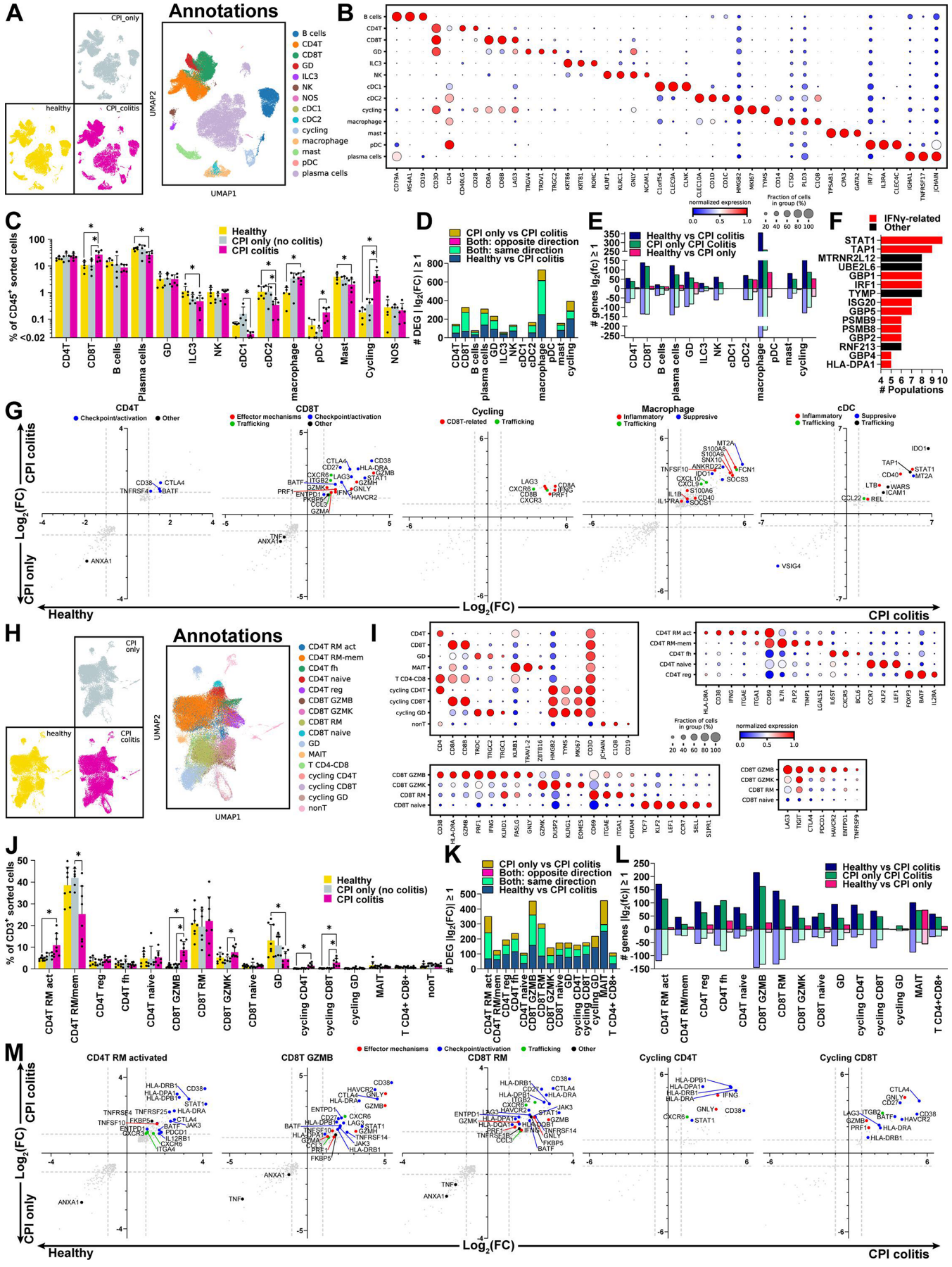

Figure 8 (Continued)

Figure 8 External validation underscores a conserved role for activated CD4 RM T cells and cDC dysregulation in CPI colitis across the steroid exposure spectrum. (A) Uniform Manifold Approximation and Projection (UMAP) plots generated from a data set of CD45$^+$-sorted colon biopsy cells, color coded by coarse annotations (right), and separately plotted by disease state in the inset at left. (B) Dot plots showing marker genes for coarse annotations. (C) Cell frequency of coarse-annotated cells by single-cell RNA sequencing in biopsies, stratified by disease states (mean+SD; each dot represents one patient; *p<0.05 and q<0.1). (D) Number of DE genes (p<0.05 and |log$_2$(FC)| >1) that are found uniquely in either healthy versus CPI colitis, CPI only (no colitis) versus CPI colitis, or both comparisons, for each coarse population. (E) Number of DE genes (p<0.05 and log$_2$(FC)>1 or <−1) between disease states, for each coarse population. (F) DE genes upregulated across the greatest number of coarse populations (p<0.05 and log$_2$(FC)>1) in both healthy versus CPI colitis and CPI only versus CPI colitis. (G) Overlapping DE genes (p<0.05 and log$_2$(FC)>1 or <−1) in both healthy versus CPI colitis (x axis) and CPI only versus CPI colitis (y axis) in select coarse populations, with genes of interest labeled. (H) UMAP plots generated from a data set of CD3$^+$-sorted colon biopsy cells, color coded by coarse annotations (right), and separately plotted by disease state in the inset at left. (I) Dot plots showing landmark genes for coarse T-cell annotations (top left), CD4$^+$ T-cell subpopulations (top right), and CD8$^+$ T-cell subpopulations (bottom left). Expression of immunotherapy targets additionally shown in CD8$^+$ T-cell subsets (bottom right). (J) Cell frequency of T-cell subpopulations out of all annotated T cells, stratified by disease states (formatted as in C). (K) Number of DE genes that are found uniquely in either healthy versus CPI colitis, CPI only (no colitis) versus CPI colitis, or both comparisons, for each T-cell subpopulation. (L) Number of DE genes between disease states, for each T-cell subpopulation. (M) Overlapping DE genes in both healthy versus CPI colitis (x axis) and CPI only versus CPI colitis (y axis) in select T-cell subpopulations, with genes of interest labeled. cDC1, conventional type 1 dendritic cells; CPI, checkpoint inhibitors; DE, differentially-expressed; ILC3, type 3 innate lymphoid cells; NK, natural killer; NOS, not otherwise specified; pDC, plasmacytoid dendritic cell; RM, resident memory; GD, gamma delta.

Separate subclustering of CD8$^+$ T cells further identifies an RM population that is *CD69*$^+$ *ITGAE*$^+$ *ITGA1*$^+$, and within the CD4$^+$ population further identifies a predominant RM population ("CD4T RM act") that co-expresses the activation markers *CD38* and *HLA-DRA* as in our data, with a separate population that does not express these markers and has mixed features of RM and memory cells ("CD4T RM-mem") (figure 8I). Importantly, in addition to enrichment of *GZMB*$^+$ CD8$^+$ and cycling T cells, CPI colitis tissue also demonstrates a significant enrichment of the activated *CD38*$^+$ *HLA-DRA*$^+$ CD4$^+$ RMs that is not an effect of CPI treatment alone (figure 8J). This is despite a lack of enrichment of CD8$^+$ RMs, and a significant depletion in the non-activated CD4$^+$ RM-memory population, as previously described. This argues that activated CD38$^+$ HLA-DR$^+$ CD4$^+$ RMs, which we first described in the primarily steroid-experienced CPI colitis state, may be mobilized at a low level in CPI colitis prior to steroid exposure as well. As the disease spectrum shifts to steroid-experienced or refractory colitis, further activation of this subset may result in a quantitative enrichment and further generation of cytotoxic effectors as seen in our data.

A closer examination of co-regulated genes in prominent T-cell subpopulations reveals common versus distinct regulation of activated CD4$^+$ RMs. Again, T-cell subpopulations demonstrate modules of genes that are co-regulated in CPI treatment and CPI colitis, as well as distinct genes specific to the CPI colitis state that are not seen with CPI exposure without colitis (figure 8K,L, online supplemental table S12). Comparing activated CD4$^+$ RMs versus their CD8$^+$ RM and cytotoxic CD8$^+$ *GZMB*$^+$ counterparts, common features upregulated in both CPI treatment and CPI colitis include marked overexpression of *CD38* (in contrast to its less pronounced overexpression in our mostly steroid-experienced data), as well as chemokines such as *CXCR6*, immune checkpoints such as *CTLA4* and *ENTPD1*, and activation markers such as MHC class II (figure 8M). At the same time, the activated CD4$^+$ RMs are distinct in being less cytotoxic than their CD8$^+$ counterparts, but also in their upregulation of *PDCD1* (vs *LAG3*/*HAVCR2* in CD8$^+$), the distinct integrin *ITGA2* (vs *ITGB2* in CD8$^+$ RM), and the distinct immune checkpoint *TNFRSF25* (death receptor 3). These findings require validation but point to largely conserved cell-intrinsic functional programs in the T-cell compartment in steroid-naïve and steroid-experienced states, but also separate regulatory mechanisms of activated CD4$^+$ RMs that may be useful for their identification and targeted treatment.

DISCUSSION

This unbiased discovery of immune and non-immune constituents in primarily steroid-experienced CPI colitis patients, with internal proteomic validation and external cross-validation in a steroid-naïve CPI colitis cohort, identifies several novel paradigms for further study and therapeutic targeting.

First, many immune hallmarks are similar in steroid-naïve and steroid-experienced disease across cancer types and separate collections, namely quantitative enrichment of CD8$^+$ cytotoxic T cells, myeloid-derived inflammation, depletion of cDCs and ILC3, and mobilization of IFN pathway signaling across cell types, resulting in upregulation of MHC class II expression.[2 3] Despite the limited sample size, our multiplexed design (which eliminates contributions of experimental batch effect), and the validation of similar changes in the immune microenvironment in the external steroid-naïve data set, increases the confidence that these are conserved features of CPI colitis regardless of steroid exposure. However, one key distinction between steroid-naïve and experienced settings may revolve around the role of RM populations. While the clonal expansion and relationship between CD8$^+$ RM and CD8$^+$ cytotoxic effectors has been described,[2 3] in

general, the CD8+ RM population has been described as unchanged or depleted in steroid-naïve disease, and how this translates to steroid-experienced or refractory disease (and other RM populations) has been unclear.

Here we document that activated RMs that co-express CD38 and HLA-DR (both the CD8+ and unexpectedly the CD4+ RM populations) are quantitatively enriched across the steroid exposure spectrum in CPI colitis, suggesting activation even at the onset of CPI colitis pathogenesis, and that in predominantly steroid-experienced samples these activated CD4+ RMs are directly clonally related to their CD8+ RM and cytotoxic counterparts. In steroid-naïve disease, however, the overall RM population abundance is not changed or is depleted, while in primarily steroid-experienced disease, both CD4+ RM and CD8+ RMs are significantly enriched. This suggests that as CPI colitis is exposed to steroids and becomes steroid refractory, there is further mobilization of both CD4+ RM and CD8+ RM precursors, leading to increased production of cytotoxic CD8+ effectors to amplify tissue damage. While the possibility of CD4+ RM precursors giving rise to CD8+ cytotoxic effectors is unexpected, cross-lineage differentiation between CD4+ and CD8+ T cells has been described within the intestinal microenvironment,[28] underscoring a putative pathogenic role for both CD4+ RM and CD8+ RM precursors. We identify distinct immune checkpoints associated with activated CD4+ RMs in CPI colitis (*PDCD1*, *ITGA2*, *TNFRSF25*) which may serve as experimental handles for their identification, isolation, and targeting to prevent amplification of immune cytotoxic mechanisms in this disease state. *TNFRSF25* may be of particular therapeutic interest in CPI colitis as antibodies targeting TL1A which binds this immune checkpoint appear to be efficacious in inflammatory bowel disease (IBD).[29] While other investigators have documented enrichment of CD38+ HLA-DR+ CD8+ cytotoxic and RM phenotypes in CPI colitis,[4] this has not been described for CD4+ RMs, and the deeper characterization of these CD38+ HLA-DR+ T-cell subsets at single-cell resolution had not been completed before this study. CD38 and HLA-DR may have separate functional roles in CPI colitis pathogenesis, for example, through NAD+ depletion[30] or direct antigen presentation by non-professional, non-immune HLA-DR+ populations, respectively.

We highlight key distinctions between mechanisms of colitis induced by αPD-1 and αCTLA-4 (in combination with αPD-1). In the T-cell compartment, the effects of αCTLA-4 include enrichment of *ITGB2*+ CD8+ T cells which have been postulated to circulate[3] but also include co-stimulation, upregulation of immune checkpoints, and myeloid-related inflammation which are consistent with broader priming of multiple arms of immunity as well as re-circulation of pathogenic effectors. On the other hand, our findings with αPD-1 colitis point to a narrower T cell-driven program that involves a cytotoxic program, and distinct integrins (eg, *ITGAE*, *ITGB7*). This is consistent with pathologic findings of a lymphocytic colitis often associated with αPD-1 colitis. Due to patient heterogeneity and limited sample size, these findings are hypothesis-generating and require validation in other data sets, as well as steroid-naïve disease, but indicate the possibility of distinct integrin targeting within the T-cell compartment for αPD-1 colitis, and broader myeloid targeting for αCTLA-4 colitis.

Our study also underscores the contribution of non-immune stromal populations to CPI colitis. This has been limited to date as several prior surveys focused on the collection and study of immune cells.[2] The finding of conserved dysregulation of NAD+ and tryptophan metabolism in stromal cells as well as cDC2s, validated for cDCs in steroid-naïve disease, is further enhanced by our ability to internally compare with UC samples in the same multiplexed design. That these pathways are particularly upregulated in CPI colitis in direct comparisons to UC nominates these as promising therapeutic targets. An important limitation in the CPI versus UC comparison is the limited sample size (n=2 UC biopsies with single cells from the multiplexed experiment), also these two UC patients had less active disease at the time of collection (endoscopic severity score 0), which may lead to overestimation of the difference between CPI and UC immunopathology. Despite that caveat, we separately embarked on a larger comparison of UC versus HC, multiplexed using the same methodology, and did not find significant enrichment of T cells in UC,[5] in contrast to our findings of enriched RM and cytotoxic effector T cells in CPI colitis, supporting the idea that these are distinct colitis states and that CPI colitis is more mechanistically driven by pathogenic T cells, as we describe in this work.

There are several important limitations of this study. We chose to focus primarily on host factors involved in CPI colitis, although the microbiome plays central roles in tumor immunotherapy response and CPI colitis.[31 32] This study captures a wide spectrum of the variability in the CPI colitis disease course, identifying common pathways independent of tumor type and CPI. Future studies with larger numbers of patients will be necessary to assess the contributions of tumor type, CPI treatment, and immunosuppression. The UC patients included in this study were also heterogeneous, and additional studies will be necessary to comprehensively compare and contrast CPI colitis with UC, Crohn's disease, and microscopic colitis.

Finally, we demonstrate the importance of studying the dysregulation of current therapeutic targets in the CPI colitis state, through our demonstration of endothelial upregulation of the MAdCAM-1 ligand for α4β7 integrin. While this interaction is currently targeted in the clinic, via off-label use of vedolizumab extrapolated from IBD, it remains unclear which patients would best benefit from this therapy, and whether vedolizumab should be given before or after TNF blockade, or after specific types of CPI. We nominate patients with αCTLA-4 induced colitis, and those who have previously experienced TNF blockade, as those who might particularly upregulate MAdCAM-1 across patients and may have added benefit. One recent

study highlighted the importance of MAdCAM-1 in mediating responsiveness to immunotherapy and proposed soluble MAdCAM-1 as a potential biomarker.[31] Here we show that endothelial expression of *MADCAM1* may also be relevant as a biomarker for CPI colitis. While this approach requires validation in larger cohorts of patients, it also shows the promise of unbiased discovery of known and novel trafficking targets, to complement and guide ongoing experimentation in the clinic such as ongoing randomized trials of vedolizumab versus TNF blockade (infliximab) for steroid-experienced CPI colitis patients (eg, NCT04407247).[33]

METHODS

Study participants and biospecimen collection

Patients undergoing colonoscopy or sigmoidoscopy for standard-of-care indications were screened for study eligibility. Peripheral blood and cold forceps biopsy samples were obtained from patients with CPI colitis, UC, and individuals without IBD as "healthy controls" (HC). HC patients were patients without known or suspected IBD undergoing elective colonoscopy or sigmoidoscopy for various indications (eg, colorectal cancer screening). Biopsies were obtained from the left (distal) colon. Biopsies were placed in Basal Organoid Media consisting of advanced DMEM/F12 with NEAA and Sodium Pyruvate (Thermo Fisher Scientific) supplemented with HEPES (10 mM, Corning),GlutaMAX (2 mM, Thermo Fisher Scientific), Normocin (100 µg/mL, Invivogen ant-nr-2), Penicillin-Streptomycin-Neomycin (Thermo Fisher Scientific), and N-acetylcysteine (1 mM, Millipore Sigma), supplemented with Y-27632 (10 µM, MedChemExpress). Samples were immediately placed on ice and transported to the laboratory for processing as previously described.[34]

Sample collection and storage

Colon biopsies were obtained with endoscopic biopsy forceps from the left colon for pathologic confirmation of disease. For samples that were taken for research: biopsies were collected in RNA later in a 5 mL tube, and stored overnight at 4°C. Then solution was aspirated and biopsies were stored at −70°C until further analysis. In some cases, additional biopsies were collected in 10% formalin in 5 mL tubes for 24 hours, then washed with phosphate-buffered saline (PBS) twice and stored in 70% ethanol for paraffin embedding. Biopsies were collected in a conical tube with Basal Media (Advanced DMEM/F12 with NEAA and Sodium Pyruvate, Thermo cat. No. 12 634–010; 2 mM GlutaMAX, Thermo cat. No. 35050061; 10 mM HEPES (Corning); Penicillin-Streptomycin-Neomycin Antibiotic Mixture, Thermo cat. No. 15640055; Normocin 100 µg/mL, Invivogen cat. No. ant-nr-2; 1 mM N-acetylcysteine, Sigma-Aldrich, A9165) with 10 µM Y-27632 (MedChemExpress) at 4°C and then transferred into cryovials containing freezing media (90% (v/v) fetal calf serum (FCS), 10% (v/v) dimethyl sulfoxide (DMSO) and 10 µM Y-27632) and immediately placed into a freezing container (Mr Frosty or Coolcell) and stored at −70°C for up to 4 weeks before transferring to liquid nitrogen cryostorage until further processing. For some samples, a PAXgene RNA tube (Qiagen) was collected, stored, and processed according to the manufacturer's instructions. For peripheral leukocyte isolation, in brief, peripheral blood was collected into Ethylenediaminetetraacetic acid (EDTA) tubes (BD, 366643). 2 mL aliquots of peripheral blood were treated with 30 mL of RBC lysis buffer (Roche) for 5–8 min at room temperature (RT) with gentle mixing. Cells were resuspended in CryoStor CS10 (at 4°C) freezing medium, aliquoted in cryovials, transferred to a freezing container (Mr Frosty or Coolcell), and stored at −70°C for up to 4 weeks before transferring to liquid nitrogen cryostorage until further processing.

Preparation of colon and peripheral blood single-cell suspensions

Colon biopsies were thawed for 2 min with gentle agitation in a 37°C water bath, transferred to a gentleMACS C Tube (Miltenyi Biotec), washed twice with basal media containing 10 µM Y-27632, and then incubated in 5 mL digestion buffer (basal media, 10 µM Y-27632, 600 U/mL collagenase IV (Worthington cat. No. LS004189), 0.1 mg/mL DNAse I (Sigma-Aldrich, D4513) and digested for 20 min at 37°C in a shaking incubator set at 225 rpm. Subsequently, samples were placed in the gentleMACS dissociator and run the gentleMACS Program m_intestine_01 followed by 15 min incubation at 37°C in a shaking incubator set at 225 rpm. The suspension was then strained through a 100 µm strainer (Miltenyi) and centrifuged at 450 x g for 5 min at RT. Two additional washes were performed in Hanks' Balanced Salt Solution (HBSS) (Corning), containing 0.1 mg/mL DNAse I (Sigma-Aldrich, D4513). 1×10^6 total cells were set aside for CyTOF. For the remaining cells, dead cells were removed with the Dead Cell Removal Kit (Miltenyi) according to the manufacturer's instructions. Cell suspensions were counted using a TC20 Automated Cell Counter (Bio-Rad) with 0.4% Trypan Blue Solution (Thermo Fisher Scientific). Live-cell enriched colon single-cell suspensions were used for scRNA-seq and CITE-seq, with a final pooled viability was >75%. Peripheral blood leukocytes were thawed for 2 min with gentle agitation in a 37°C water bath and then washed twice with complete DMEM (Thermo Fisher) supplemented with non-essential amino acids (Thermo Fisher Scientific), sodium pyruvate (Thermo Fisher Scientific), HEPES (10 mM; Corning), GlutaMAX (2 mM; Thermo Fisher Scientific), Normocin (100 µg/mL; Invivogen, ant-nr-2), penicillin–streptomycin (Thermo Fisher Scientific) and 10% fetal bovine serum (VWR). Cells were incubated with ACK lysis buffer (Quality Biological) for 5 min at room temperature, washed twice with complete DMEM, treated with HBSS (Corning), containing 0.1 mg/mL DNAse I (Sigma-Aldrich, D4513) for 5 min, and then strained through a 20 µm pre-separation filter (Miltenyi). Cells were counted using a TC20 Automated Cell Counter (Bio-Rad) with 0.4% Trypan Blue Solution

(Thermo Fisher Scientific). Peripheral blood leukocytes from each donor were used for scRNA-seq and CyTOF, with a final pooled viability of >85%.

Bulk RNA sequencing sample and computational processing

RNA was extracted from blood or biopsies following the manufacturer's protocol using PAXgene kit and Qiagen RNeasy Mini kit (Qiagen), respectively. RNA quality and integrity were measured with the Agilent RNA 6000 Nano Kit on the Agilent 2100 Bioanalyzer, according to the manufacturer's instructions. Ribosomal and hemoglobin-depleted total RNA sequencing libraries were created using FastSelect (Qiagen cat#: 335377) and Tecan Universal Plus mRNA-Seq (0520-A01) with adaptations for automation of a Beckman Biomek FX^P system. Libraries were subsequently normalized and pooled for Illumina sequencing using a Labcyte Echo 525 system available at the Center for Advanced Technology at University of California, San Francisco (UCSF). The pooled libraries were sequenced on an Illumina NovaSeq S4 flow cell lane with paired-end 150 bp reads. Computation processing for genotyping was performed as previously described.[35 36] Briefly, sequencing reads were aligned to the human reference genome and Ensembl annotation (GRCh38 genome build, Ensembl annotation V.95) using STAR V.2.7.5c (PMID: 23104886) with the following parameters: –outFilterType BySJout –outFilterMismatchNoverLmax 0.04 – outFilterMismatchNmax 999 –alignSJDBoverhangMin 1 –outFilterMultimapNmax 1 – alignIntronMin 20 –alignIntronMax 1000000 –alignMatesGapMax 1 000000. Duplicate reads were removed and read groups were assigned by individual for variant calling using Picard Tools V.2.23.3 (http://broadinstitute.github.io/picard/). Nucleotide variants were identified from the resulting bam files using the Genome Analysis Tool Kit (V.4.0.11.0) following the best practices for RNA sequencing variant calling.[37] This includes splitting spliced reads, calling variants with HaplotypeCaller (added parameters: –do not-use-soft-clipped-bases-standcall-conf 20.0), and filtering variants with VariantFiltration (added parameters: -window 35 – cluster 3 –filter-name FS -filter FS>30.0 –filter-name QD -filter QD<2.0). Variants were further filtered to include a list of high-quality single-nucleotide polymorphisms (SNPs) for identification of the subject of origin of individual cells by removing all novel variants, maintaining only biallelic variants with MAF greater than 5%, a mix missing of one individual with a missing variant call at a specific site and requiring a minimum depth of two (parameters: –max-missing 1.0 –min-alleles 2 –max-alleles 2 –removeindels –snps snp.list.txt –min-meanDP 2 –maf 0.05 –recode –recode-INFO-all –out).

scRNA-seq and CITE-seq sample loading and sequencing

PBMC or colon single-cell suspensions from each patient were pooled respectively with an equivalent number of live cells and resuspended at 1–2.5×10^3 cells/µL in 0.04% bovine serum albumin (BSA)/PBS, with the addition of 10 µM Y-27632 (MedChemExpress), so that each sample could later be uniquely identified using demuxlet.[6] 1×10^6 cells of both single-cell PBMC and colon suspension pools were stained with a custom TotalSeq-C panel (BioLegend, online supplemental table S2) according to the manufacturer's instructions. The two pools were loaded into four wells, 60,000 cells per well, and processed for single-cell encapsulation and complementary DNA library generation using Chromium Single Cell 5' v2 Reagent Kits (10x Genomics), TotalSeq-C library generation was performed according to manufacturer's instructions (BioLegend). Libraries were sequenced on an Illumina NovaSeq6000 in order to obtain 25,000 reads per cell for the gene expression libraries and 10,000 reads per cell for the TotalSeq libraries.

scRNA-seq and CITE-seq data pre-processing, inter-sample doublet detection, and demuxlet

10x Genomics Chromium scRNA-seq data were processed as previously described.[35 36] Briefly, sequencer-obtained bcl files were demultiplexed into individual library fastq trios using the mkfastq program from theCell Ranger V.3.0.2 suite of tools (https://support.10xgenomics.com). Feature-barcode matrices were obtained for each sample by aligning the raw fastqs to GRCh38 reference genome (annotated with Ensembl V.85) using the Cellranger count. Raw feature-barcode matrices were loaded into Seurat V.3.1.5[38] and low-quality cells (with fewer than 100 features), and features in three or fewer cells were dropped from the data set. The remaining events were assessed for inter-sample doublet detection (generated due to libraries containing samples pooled prior to loading) using Freemuxlet (https://github.com/statgen/popscle), the genotype-free version of demuxlet.[6] Clusters of cells belonging to the same patient were identified via SNP concordance to a "truth set" generated by bulk RNA-seq. Briefly, the aligned reads from Cell Ranger were filtered to retain reads overlapping a high-quality list of SNPs obtained from the 1000 Genomes Consortium (1 KG).[39] Freemuxlet was run on this filtered bam using the 1 KG vcf file as a reference, the input number of samples/pool as a guideline for clustering groups of cells by SNP concordance, and all other default parameters. Cells are classified as singlets (arising from a single library), doublets (arising from two or more libraries), or as ambiguous (cells that cannot be accurately assigned to any existing cluster due to a lack of sufficient genetic information). Clusters of cells belonging to a unique sample were mapped to patients using their individual Freemuxlet-generated genotype, and ground truth genotypes per patient identified via bulk RNA-seq. The pairwise discordance between inferred and ground-truth genotypes was assessed using the bcftools gtcheck command.[40] The feature-barcode Matrices were further filtered to remove cells with greater than 50% mitochondrial content or ribosomal content, and cells assigned as doublets or ambiguous by Freemuxlet. Visual outliers in the feature-versus-unique molecular identifiers (UMIs)

plots were filtered uniformly across all libraries. The cell cycle state of each cell was assessed using a published set of genes associated with various stages of human mitosis.[41]

scRNA-seq and CITE-seq quality control, normalization, and intrasample heterotypic doublet detection

The filtered count matrices were normalized, and variance was stabilized using negative binomial regression via the scTransform method offered by Seurat.[42] The effects of mitochondrial content, ribosomal content, and cell cycle state were regressed out of the normalized data to prevent any confounding signal. The normalized matrices were reduced to a lower dimension using principal component analyses (PCA) and the first 30 principal coordinates per sample were subjected to a non-linear dimensionality reduction using UMAP. Clusters of cells sharing similar transcriptomic signals were initially identified using the Louvain algorithm, and clustering resolutions varied between 0.6 and 1.2 based on the number and variety of cells obtained in the data sets. All libraries were further processed to identify intrasample heterotypic doublets arising from the 10× sample loading. Processed and annotated Seurat objects were processed using the DoubletFinder package.[43] The prior doublet rate per library was approximated using the information provided in the 10× knowledgebase (https://kb.10xgenomics.com/hc/en-us/articles/360001378811) and this was corrected to account for intersample doublets identified by Freemuxlet, and for homotypic doublets using the per-cluster numbers in each data set. Heterotypic doublets were removed. The raw and log-normalized counts per library were then pruned to retain only genes shared by all libraries. Pruned counts matrices were merged into a single Seurat object and the batch (or library) of origin was stored in the metadata of the object. The log-normalized counts were reduced to a lower dimension using PCA and the individual libraries were aligned in the shared PCA space in a batch-aware manner (each individual library was considered a batch) using the Harmony algorithm.[44] The resulting Harmony components were used to generate batch-corrected UMAP visualizations and cell clustering.

scRNA-seq and CITE-seq cell annotation and differential expression

For both blood and biopsy scRNA-seq and CITE-seq, we generated h5ad files with the UMAP, Louvain clusters, and metadata. We then refined the “coarse” and “fine” cell-type annotations in a semi-supervised manner using exploratory CELLxGENE (ExCellxGene) (https://pypi.org/project/excellxgene/), a restructured version of CELLxGENE.[45] Expression of cell-type specific markers was used to assign identities to “coarse” and “fine” clusters, guided by previously described gene sets.[46–50] scRNA-seq and CITE-seq data analysis and visualization were then performed in Jupyter notebooks using Scanpy.[51] Changes in cell frequencies were calculated as a per cent of total cells for coarse-annotated populations, or as a per cent of parent-population for fine-annotated cells. Significant differences in cell-frequencies was tested using Mann-Whitney test for comparison of two groups or the Kruskal-Wallis test for the comparison of three groups. Afterwards, using the p values from comparisons that share a denominator when calculating frequencies, we analyzed a stack of p values using the two-stage linear step-up procedure of Benjamini, Krieger and Yekutieli with false discovery rate (Q)=10%. To compute DE genes between two conditions, we first subsetted our data sets with a pair of conditions (HC vs UC, HC vs CPI colitis, UC vs CPI colitis; HC vs PD-1, HC vs combo, PD-1 vs combo; HC vs steroid, HC vs TNF, steroid vs TNF; HC vs CPI colitis, no colitis vs CPI colitis, HC vs no colitis). Then, we used the MAST R package V.1.20 which implements a negative-binomial model using the zlm method and corrects for differences in sequencing depth across samples.[52] Briefly, for a subsetted data set of two conditions, we subsetted again for each cell type (coarse annotation for biopsies, and fine annotation for blood) to identify DE genes for each cell type between the two conditions. We also corrected for the number of detected genes as a potential confounding variable.[52] P values were corrected using the Bonferroni correction.

Third-party scRNA-seq data set preprocessing

Published scRNA-seq data sets of $CD45^+$ or $CD3^+$-sorted patient biopsy cells from steroid-naïve CPI colitis patients and controls (CPI treatment but no colitis, HC) were downloaded from Gene Expression Omnibus under accession number: GSE144469.[2] Both data sets were processed in Jupyter notebooks using Scanpy.[51] We ran Scrublet (https://github.com/swolock/scrublet) to remove predicted doublets. We applied the following cut-offs to filter for high-quality cells: <10% mitochondrial genes, >100 and <4,000 genes expressed per cell, and excluded platelets, red blood cells, and doublets. We filtered out ribosomal genes and genes detected in less than three cells. We log-transformed, normalized the data to 10,000 counts per cell, per cent mitochondrial genes, and a number of gene counts, and scaled genes to unit variance. We filtered on highly variable genes and ran the principal component analysis with Scanpy. We performed batch correction using Harmony (https://github.com/hbctraining/scRNA-seq_online). We computed a neighborhood graph of observations, performed Leiden clustering, and generated a UMAP using Scanpy. Afterwards, scRNA-seq cell annotation, frequency calculation, and differential expression testing were performed as described above. For DE testing by MAST, the sign of the results were inverted to remain consistent with the direction of DE testing in our predominantly steroid-experienced object.

Mass cytometry sample staining and acquisition

A 37-parameter CyTOF panel was designed (online supplemental table S2). All mass cytometry antibodies were conjugated in-house to their corresponding metal

isotope. Metals were conjugated according to the manufacturer's instructions (Fluidigm, South San Francisco, California, USA). In brief, this process consisted of loading the metal to a polymer for 1 hour at RT. The unconjugated antibody is transferred into a 50 kDa Amicon Ultra 500 V-bottom filter (Fisher Scientific, Hampton, New Hampshire, USA) and reduced for 30 min at 37°C with 1:125 dilution of Tris (2-carboxyethyl) phosphine hydrochloride (Thermo Fisher, Waltham, Massachusetts, USA). Subsequently, the column was washed twice with C-buffer (Fluidigm) and the metal-loaded polymer was suspended in 200 µL of C-buffer in the 3 kDa Amicon Ultra 500 mLV-bottom filter. The suspension was transferred to the 50 kDa filter containing the antibody and incubated for 1.5 hours at 37°C. After incubation, antibodies were washed three times with W-buffer (Fluidigm) and quantified for protein content using NanoDrop. Once the concentration was determined the antibodies were resuspended at a concentration of 0.2 mg/mL with Antibody Stabilizer (Boca Scientific, Dedham, Massachusetts, USA) and stored at 4°C. Optimal concentrations for all antibodies were determined by different rounds of titrations. The staining protocol was optimized to use each antibody in aliquots of 6 million cells as previously described.[53]

Mass cytometry panel design, staining, and acquisition

Mass cytometry was performed on biopsies from the left colon. Dead cells were labeled with Cisplatin (Fluidigm) according to the manufacturer's instructions, washed in fluorescence-activated cell sorting (FACS) buffer, and then stored at −80°C until staining. Samples were then thawed and washed with wash buffer (PBS, 0.5% BSA, 5mM EDTA), fixed in 1.6% paraformaldehyde (PFA) for 10 min, washed in wash buffer and then resuspended in freezing medium (PBS, 0.5% BSA, 10% DMSO) and stored at −80 C until staining. Prior to staining with the antibody panel (online supplemental table S2), cells from each patient were thawed, washed with wash buffer, and barcoded using a unique set of metals, enabling sample identification as previously described.[54 55] The barcode staining was performed following the manufacturer's instructions (Fluidigm, South San Francisco, California, USA). Briefly, each sample was incubated for 15 min at RT on a shaker (200 rpm) with a barcoding solution containing 10 µL of barcode in 1× Perm Buffer solution (Fluidigm, Cat#201057) diluted in cell staining media (CSM, Fluidigm, Cat#201068). Samples were then washed, centrifuged, resuspended in CSM, and pooled. Subsequently, extracellular staining was performed for 30 min at 4°C. After incubation, the samples were washed with CSM and centrifuged before resuspending in 1× Permeabilization Buffer (eBioscience Permeabilization Buffer Cat# 00-8333-56) for 10 min at 4°C. The samples were then washed and incubated with Ir-intercalator (BioLegend CNS, San Diego, California, USA) diluted 1:500 in 4% fresh paraformaldehyde (PFA) for 20 min at RT. After incubation, samples were washed and kept at 4°C overnight in EQ bead solution (Fluidigm Cat#201078) diluted in Maxpar Water (Fluidigm Cat# 201069) at 1.2×10^6 cells/mL. Samples were analyzed on the CyTOF2 instrument (Fluidigm).

Mass cytometry data analysis

After acquisition, the .fcs files obtained were concatenated, normalized to the EQ calibration beads, and de-barcoded using CyTOF software (Fluidigm). FlowJo software was used for confirming the elimination of the EQ calibration beads, concatenating, and manually gating the files. Singlets were gated by event length and DNA. Live cells were identified as cisplatin-negative. The unsupervised analysis was performed using an R-based Cytometry Clustering Optimization aNd Evaluation (Cyclone) pipeline developed by UCSF Data Science CoLab (https://github.com/UCSF-DSCOLAB/cyclone).[27] Specifically, the data were preprocessed, ArcSinh transformed (cofactor 5), then clustered using FlowSOM.[56] We used default values for FlowSOM parameters except for the grid size. A grid size of "2×11" was chosen based on the lower Davies-Bouldin Index. The clustering was visualized using UMAP, which was calculated using uwot package in R. The median expression levels of each of the 37 antibodies for each cluster were used to annotate clusters. This was plotted as a heatmap. Feature plots for each marker were also used to plot the expression of each marker on UMAPs. In parallel, supervised analysis was performed on the same data set defining cell subsets based on canonical markers. Finally, specific populations and markers of the focused panel were manually gated to validate and extend the results from the unsupervised analysis.

Network scRNA-seq and TCR-seq analysis

We conducted TCR network analysis at the cell level by using the R package NAIR (available at https://cran.r-project.org/web/packages/NAIR/index.html).[11] Briefly, for each patient, we calculated the pairwise Levenshtein distances between the CDR3 amino acid sequences of the alpha and beta chains in combined blood and biopsy to derive the distance matrix. Only TCRs that exhibited identical amino acid sequences in both the alpha and beta chains were linked (distance=0). Visualization of the network analysis was accomplished using the R packages igraph and graph.

Gene Set Enrichment Analysis

We performed GSEA in Jupyter notebooks using GSEApy[57] (V.1.1.1). For coarse and fine populations of interest, we used MAST-calculated DE genes with $p<0.05$ and either log2FC>1 or <−1 for upregulated or downregulated pathways respectively, between HC versus CPI colitis. We inputted the up or downregulated genes of each cell population into the gseapy.enrichr function and used "Reactome_2022" as our reference database. We then selected enriched pathways with adjusted $p<0.05$ and graphed the top 10 most significant for each population. We additionally displayed a manual curation of pathways of interest with $p<0.05$ via heatmap.

Author affiliations
[1]Division of Hematology/Oncology, Department of Medicine, University of California, San Francisco, San Francisco, California, USA
[2]Chan Zuckerberg Biohub, San Francisco, California, USA
[3]Division of Gastroenterology, Department of Medicine, University of California, San Francisco, San Francisco, CA, USA
[4]CoLabs, University of California, San Francisco, San Francisco, California, USA
[5]Department of Pathology, University of California, San Francisco, San Francisco, California, USA
[6]ImmunoX Initiative, University of California, San Francisco, San Francisco, California, USA

X Arjun A Rao @arrkal

Acknowledgements We thank the patients for their participation in these studies; the UCSF Gastroenterology providers involved in screening, enrollment, and clinical care of these patients; the UCSF Biospecimen Resources Program for assistance with tissue acquisition; the Institute for Human Genetics Core at UCSF, the UCSF Genomics CoLabs, and the UCSF Center for Advanced Technology for assistance with sequencing; and the UCSF Parnassus Flow Cytometry CoLab for assistance with BD Aria Fusion cell sorter and BD LSRFortessa cell analyzer. Schematics created with Biorender.com.

Contributors Conceptualization: ACo, MGK, DYO. Methodology: ACo, MGK, DYO. Software: JYH, Y-JK, EM, AAR, CA, KL, HY, LZ, AP, MGK, DYO. Validation: JYH, Y-JK, EM, KL, HY, LZ, AP, MGK, DYO. Formal Analysis: JYH, Y-JK, EM, AR, CA, KL, HY, AS, LZ, AP, MGK, DYO. Investigation: JYH, IR, JB, JT, AS, BD, DK, YS, FF, ACh, LF, ACo, MGK, DYO. Resources: AR, LZ, LF, ACo, AP, MGK, DYO. Data Curation: JYH, Y-JK, MGK, DYO. Writing—original draft: JYH, DYO. Writing—review and editing: JYH, EM, MGK, DYO. Visualization: JYH, Y-JK, EM, MGK, DYO. Supervision: MGK, DYO. Project Administration: MGK, DYO. Funding Acquisition: MGK, DYO. Guarantor: DYO.

Funding This study was supported by a CoPilot award from the UCSF ImmunoX initiative, the Parker Institute for Cancer Immunotherapy, and the UCSF Office of Research (for support to the UCSF CoLabs). LF was supported by a grant from the National Institutes of Health (R35CA253175). DYO was supported by an anonymous donation to the UCSF Helen Diller Family Comprehensive Cancer Center, grants from the National Institutes of Health (K08AI139375), the Damon Runyon Clinical Investigator Award (CI 110-21), and the V Foundation Translational Adult Cancer Award (T2023-011). MGK was supported by a Career Development Award from the Crohn's and Colitis Foundation and NIH K08DK123202, funding from the Kenneth Rainin Foundation, and he holds a Career Award for Medical Scientists from the Burroughs Wellcome Fund.

Competing interests DYO has received research support from Merck, PACT Pharma, the Parker Institute for Cancer Immunotherapy, Poseida Therapeutics, TCR2 Therapeutics, Roche/Genentech, and Nutcracker Therapeutics; travel and accommodations from Roche/Genentech; and has consulted for Revelation Partners. LF has received research support from Roche/Genentech, AbbVie, Bavarian Nordic, Bristol Myers Squibb, Dendreon, Janssen, Merck, and Partner Therapeutics; and has served on scientific advisory boards for Actym, AstraZeneca, Atreca, Bioatla, Bolt, Bristol Myers Squibb, Daiichi Sankyo, Immunogenesis, Innovent, Merck, Merck KGA, Nutcracker, RAPT, Scribe, Senti, Sutro, and Roche/Genentech. The Combes laboratory has received research support from Eli Lilly and Genentech and AC consults for Foundery Innovations. The Kattah laboratory receives research support from Eli Lilly, and MGK has consulted for Sonoma Biotherapeutics and Morphic Therapeutic.

Patient consent for publication Not applicable.

Ethics approval This study involves human participants and was approved by University of California, San Francisco Institutional Review Board (#19-27302, 15-16385). Participants gave informed consent to participate in the study before taking part.

Provenance and peer review Not commissioned; externally peer reviewed.

Data availability statement Data are available in a public, open access repository. All code and processed datasets used in this study are available as provided below. Processed data are deposited as a GEO Super Series under accession code GSE253723 and are publicly available.[58] Processed and annotated objects are saved in AnnData (h5ad) format on Figshare: biopsies RNA and RNA/ADT objects https://doi.org/10.6084/m9.figshare.24668922.v1; blood RNA and RNA/ADT objects https://doi.org/10.6084/m9.figshare.24668916.v1; Luoma CD45-sorted and CD3-sorted RNA objects https://doi.org/10.6084/m9.figshare.24668925.v1. Biopsy CyTOF files can be found at https://doi.org/10.6084/m9.figshare.24668934.v1. Jupyter notebooks for preprocessing of Luoma scRNAseq datasets and CLR transformation of CITEseq data; and scripts for generating UMAPs, dotplots, and heatmaps, converting h5ad to robj, MAST analysis, and GSEA analysis can be found at https://github.com/mkattah/ICI_colitis.

ORCID iDs
Alexander Cheung http://orcid.org/0000-0002-2115-6966
David Y Oh http://orcid.org/0000-0002-3310-0994

REFERENCES

1 Bellaguarda E, Hanauer S. Checkpoint inhibitor-induced colitis. *Am J Gastroenterol* 2020;115:202–10.
2 Luoma AM, Suo S, Williams HL, *et al*. Molecular pathways of colon inflammation induced by cancer immunotherapy. *Cell* 2020;182:655–71.
3 Thomas MF, Slowikowski K, Manakongtreecheep K, *et al*. Altered interactions between circulating and tissue-resident CD8 T cells with the colonic mucosa define colitis associated with immune checkpoint inhibitors. *bioRxiv* [Preprint] 2021.
4 Sasson SC, Slevin SM, Cheung VTF, *et al*. Interferon-gamma-producing CD8+ tissue resident memory T cells are a targetable hallmark of immune checkpoint inhibitor-colitis. *Gastroenterology* 2021;161:1229–44.
5 Mennillo E, Kim YJ, Lee G, *et al*. Single-cell and spatial multi-omics highlight effects of anti-integrin therapy across cellular compartments in ulcerative colitis. *Nat Commun* 2024;15:1493.
6 Kang HM, Subramaniam M, Targ S, *et al*. Multiplexed droplet single-cell RNA-sequencing using natural genetic variation. *Nat Biotechnol* 2018;36:89–94.
7 Kurachi M, Barnitz RA, Yosef N, *et al*. The transcription factor BATF operates as an essential differentiation checkpoint in early effector CD8+ T cells. *Nat Immunol* 2014;15:373–83.
8 Cho H-S, Ha S, Shin HM, *et al*. CD8+ T cells require ITK-mediated TCR signaling for migration to the intestine. *Immunohorizons* 2020;4:57–71.
9 Yang YH, Song W, Deane JA, *et al*. Deficiency of annexin A1 in CD4+ T cells exacerbates T cell-dependent inflammation. *J Immunol* 2013;190:997–1007.
10 Tangye SG. Staying alive: regulation of plasma cell survival. *Trends Immunol* 2011;32:595–602.
11 Yang H, Cham J, Neal BP, *et al*. NAIR: network analysis of immune repertoire. *Front Immunol* 2023;14:1181825.
12 Bustamante S, Yau Y, Boys V, *et al*. Tryptophan metabolism 'Hub' gene expression associates with increased inflammation and severe disease outcomes in COVID-19 infection and inflammatory bowel disease. *Int J Mol Sci* 2022;23:14776.
13 Chen C, Yan W, Tao M, *et al*. NAD+ metabolism and immune regulation: new approaches to inflammatory bowel disease therapies. *Antioxidants (Basel)* 2023;12:1230.
14 Nguyen TTT, Yoon HK, Kim YT, *et al*. Tryptophanyl-tRNA synthetase 1 signals activate TREM-1 via TLR2 and TLR4. *Biomolecules* 2020;10:1283.
15 Jin M. Unique roles of tryptophanyl-tRNA synthetase in immune control and its therapeutic implications. *Exp Mol Med* 2019;51:1–10.
16 Xie Z, Zhou G, Zhang M, *et al*. Recent developments on BMPs and their antagonists in inflammatory Bolwe diseases. *Cell Death Discov* 2023;9:210.
17 Hu L, Xu J, Wang X, *et al*. Bone morphogenetic protein 4 alleviates DSS-induced ulcerative colitis through activating intestinal stem cell by target ID3. *Front Cell Dev Biol* 2021;9:700864.

18 Takabayashi H, Shinohara M, Mao M, *et al*. Anti-inflammatory activity of bone morphogenetic protein signaling pathways in stomachs of mice. *Gastroenterology* 2014;147:396–406.
19 McCarthy N, Manieri E, Storm EE, *et al*. Distinct mesenchymal cell populations generate the essential intestinal BMP signaling gradient. *Cell Stem Cell* 2020;26:391–402.
20 Isono K, Nemoto K, Li Y, *et al*. Overlapping roles for homeodomain-interacting protein Kinases HIPK1 and HIPK2 in the mediation of cell growth in response to morphogenetic and genotoxic signals. *Mol Cell Biol* 2006;26:2758–71.
21 Tocharus J, Tsuchiya A, Kajikawa M, *et al*. Developmentally regulated expression of mouse HTRA3 and its role as an inhibitor of TGF-beta signaling. *Dev Growth Differ* 2004;46:257–74.
22 SenBanerjee S, Lin Z, Atkins GB, *et al*. KLF2 is a novel transcriptional regulator of endothelial proinflammatory activation. *J Exp Med* 2004;199:1305–15.
23 Erle DJ, Briskin MJ, Butcher EC, *et al*. Expression and function of the Madcam-1 receptor, integrin alpha 4 beta 7, on human leukocytes. *J Immunol* 1994;153:517–28.
24 Rott LS, Briskin MJ, Andrew DP, *et al*. A fundamental subdivision of circulating lymphocytes defined by adhesion to mucosal addressin cell adhesion molecule-1. comparison with vascular cell adhesion molecule-1 and correlation with beta 7 integrins and memory differentiation. *J Immunol* 1996;156:3727–36.
25 Kiparizoska S, Murphy ME, Mattar MC. Check this out: treatment paradigms in immune-checkpoint inhibitor colitis. *Curr Opin Gastroenterol* 2023;39:43–9.
26 Fries GR, Gassen NC, Rein T. The FKBP51 glucocorticoid receptor co-chaperone: regulation, function, and implications in health and disease. *Int J Mol Sci* 2017;18:2614.
27 Patel RK, Jaszczak RG, Im K, *et al*. Cyclone: an accessible pipeline to analyze, evaluate, and optimize multiparametric cytometry data. *Front Immunol* 2023;14:1167241.
28 Lui JB, Devarajan P, Teplicki SA, *et al*. Cross-differentiation from the CD8 lineage to CD4 T cells in the gut-associated microenvironment with a nonessential role of microbiota. *Cell Rep* 2015;10:574–85.
29 Furfaro F, Alfarone L, Gilardi D, *et al*. Tl1A: a new potential target in the treatment of inflammatory bowel disease. *Curr Drug Targets* 2021;22:760–9.
30 Zeidler JD, Hogan KA, Agorrody G, *et al*. The CD38 glycohydrolase and the NAD sink: implications for pathological conditions. *Am J Physiol Cell Physiol* 2022;322:C521–45.
31 Fidelle M, Rauber C, Alves Costa Silva C, *et al*. A microbiota-modulated checkpoint directs immunosuppressive intestinal T cells into cancers. *Science* 2023;380:eabo2296.
32 Routy B, Le Chatelier E, Derosa L, *et al*. Gut microbiome influences efficacy of PD-1-based immunotherapy against epithelial tumors. *Science* 2018;359:91–7.
33 Zou F, Faleck D, Thomas A, *et al*. Efficacy and safety of vedolizumab and Infliximab treatment for immune-mediated diarrhea and colitis in patients with cancer: a two-center observational study. *J Immunother Cancer* 2021;9:e003277.
34 Rusu I, Mennillo E, Bain JL, *et al*. Microbial signals, MYD88, and lymphotoxin drive TNF-independent intestinal epithelial tissue damage. *J Clin Invest* 2022;132:e154993.
35 Combes AJ, Courau T, Kuhn NF, *et al*. Global absence and targeting of protective immune states in severe COVID-19. *Nature* 2021;591:124–30.
36 Combes AJ, Samad B, Tsui J, *et al*. Discovering dominant tumor immune archetypes in a pan-cancer census. *Cell* 2022;185:184–203.
37 Van der Auwera GA, Carneiro MO, Hartl C, *et al*. From FastQ data to high-confidence variant calls: the genome analysis toolkit best practices pipeline. *Curr Protoc Bioinformatics* 2013;43:11.
38 Stuart T, Butler A, Hoffman P, *et al*. Comprehensive integration of single-cell data. *Cell* 2019;177:1888–902.
39 Auton A, Brooks LD, Durbin RM, *et al*. A global reference for human genetic variation. *Nature* 2015;526:68–74.
40 Li H. A statistical framework for SNP calling, mutation discovery, association mapping and population genetical parameter estimation from sequencing data. *Bioinformatics* 2011;27:2987–93.
41 Dominguez D, Tsai Y-H, Gomez N, *et al*. A high-resolution transcriptome map of cell cycle reveals novel connections between periodic genes and cancer. *Cell Res* 2016;26:946–62.
42 Hafemeister C, Satija R. Normalization and variance stabilization of single-cell RNA-Seq data using regularized negative binomial regression. *Genome Biol* 2019;20:296.
43 McGinnis CS, Murrow LM, Gartner ZJ. Doubletfinder: doublet detection in single-cell RNA sequencing data using artificial nearest neighbors. *Cell Syst* 2019;8:329–37.
44 Korsunsky I, Millard N, Fan J, *et al*. Fast, sensitive and accurate integration of single-cell data with harmony. *Nat Methods* 2019;16:1289–96.
45 Jones RC, Karkanias J, *et al*, The Tabula Sapiens Consortium*. The Tabula Sapiens: a multiple-organ, single-cell Transcriptomic Atlas of humans. *Science* 2022;376:eabl4896.
46 Kinchen J, Chen HH, Parikh K, *et al*. Structural remodeling of the human colonic mesenchyme in inflammatory bowel disease. *Cell* 2018;175:372–86.
47 Parikh K, Antanaviciute A, Fawkner-Corbett D, *et al*. Colonic epithelial cell diversity in health and inflammatory bowel disease. *Nature* 2019;567:49–55.
48 Smillie CS, Biton M, Ordovas-Montanes J, *et al*. Intra- and inter-cellular rewiring of the human colon during ulcerative colitis. *Cell* 2019;178:714–30.
49 Martin JC, Chang C, Boschetti G, *et al*. Single-cell analysis of Crohn's disease lesions identifies a pathogenic cellular module associated with resistance to anti-TNF therapy. *Cell* 2019;178:1493–508.
50 Fawkner-Corbett D, Antanaviciute A, Parikh K, *et al*. Spatiotemporal analysis of human intestinal development at single-cell resolution. *Cell* 2021;184:810–26.
51 Wolf FA, Angerer P, Theis FJ. SCANPY: large-scale single-cell gene expression data analysis. *Genome Biol* 2018;19:15.
52 Finak G, McDavid A, Yajima M, *et al*. MAST: a flexible statistical framework for assessing transcriptional changes and characterizing heterogeneity in single-cell RNA sequencing data. *Genome Biol* 2015;16:278.
53 Ma T, Luo X, George AF, *et al*. HIV efficiently Infects T cells from the endometrium and remodels them to promote systemic viral spread. *Elife* 2020;9:e55487.
54 Bodenmiller B, Zunder ER, Finck R, *et al*. Multiplexed mass cytometry profiling of cellular states perturbed by small-molecule regulators. *Nat Biotechnol* 2012;30:858–67.
55 Zunder ER, Finck R, Behbehani GK, *et al*. Palladium-based mass tag cell barcoding with a doublet-filtering scheme and single-cell deconvolution algorithm. *Nat Protoc* 2015;10:316–33.
56 Van Gassen S, Callebaut B, Van Helden MJ, *et al*. Flowsom: using self-organizing maps for visualization and interpretation of cytometry data: Flowsom. *Cytometry A* 2015;87:636–45.
57 Fang Z, Liu X, Peltz G. Gseapy: a comprehensive package for performing gene set enrichment analysis in python. *Bioinformatics* 2023;39:btac757.
58 He J, *et al*. Data from: dysregulation of CD4+ and CD8+ resident memory T, myeloid, and stromal cells in steroid-experienced, checkpoint inhibitor colitis. NCBI Gene Expression Omnibus, Available: https://www.ncbi.nlm.nih.gov/geo/query/acc.cgi?acc=GSE253723